Chapter 3

The Neutrino Heating Effect

3.1 Theoretical Background

At temperatures $T \gg 20$ TK all three species of leptons and neutrinos and their corresponding antiparticles are plentiful, and in thermal equilibrium with each other. Muons and muon neutrinos come in contact with electrons and electron neutrinos through reactions such as [37]:

$$\begin{aligned}
&\mathrm{e}^- + \mu^+ \leftrightarrow \nu_\mathrm{e} + \bar{\nu_\mu} \qquad && \mathrm{e}^+ + \mu^- \leftrightarrow \bar{\nu}_\mathrm{e} + \nu_\mu \\
&\nu_\mathrm{e} + \mu^- \leftrightarrow \nu_\mu + \mathrm{e}^- \qquad && \bar{\nu_\mathrm{e}} + \mu^+ \leftrightarrow \bar{\nu_\mu} + \mathrm{e}^+ \\
&\nu_\mu + \mu^+ \leftrightarrow \nu_\mathrm{e} + \mathrm{e}^+ \qquad && \bar{\nu_\mu} + \mu^- \leftrightarrow \bar{\nu}_\mathrm{e} + \mathrm{e}^-
\end{aligned}$$

and similar reactions exist between electrons/electron neutrinos and τ particles and τ neutrinos.

$$\mathrm{e}^- + \tau^+ \leftrightarrow \nu_e + \bar{\nu_\tau} \qquad \mathrm{e}^+ + \tau^- \leftrightarrow \bar{\nu}_\mathrm{e} + \nu_\tau$$

$$\nu_{\mathrm{e}} + \tau^- \leftrightarrow \nu_\tau + \mathrm{e}^- \qquad \bar{\nu_{\mathrm{e}}} + \tau^+ \leftrightarrow \bar{\nu_\tau} + \mathrm{e}^+$$

$$\nu_\tau + \tau^+ \leftrightarrow \nu_{\mathrm{e}} + \mathrm{e}^+ \qquad \bar{\nu_\tau} + \tau^- \leftrightarrow \bar{\nu}_{\mathrm{e}} + \mathrm{e}^-$$

These reactions involve the creation and annihilation of τ particles and τ neutrinos. But 20 TK is the temperature when kT is about equal to the τ particle mass $m_\tau = 1754$ MeV. Below 20 TK the particles on the right hand sides no longer have the energy for the reactions to work in reverse. The τ particles are depleted through annihilation, and contact between τ neutrinos and electrons and positrons is lost. Muon neutrinos similarly lose contact with electrons when kT falls to around $m_\mu = 106$ MeV, at $T = 1200$ GK.

Electrons and positrons remain in contact with neutrinos via these reactions.

$$\mathrm{e}^- + \nu_i \leftrightarrow \mathrm{e}^- + \nu_i \qquad \mathrm{e}^- + \bar{\nu}_i \leftrightarrow \mathrm{e}^- + \bar{\nu}_i$$

$$\mathrm{e}^+ + \nu_i \leftrightarrow \mathrm{e}^+ + \nu_i \qquad \mathrm{e}^+ + \bar{\nu}_i \leftrightarrow \mathrm{e}^+ + \bar{\nu}_i$$

$$\mathrm{e}^- + \mathrm{e}^+ \leftrightarrow \nu_i + \bar{\nu}_i$$

When $T = 6$ GK kT is equal to $m_{\mathrm{e}} = 0.511$ MeV. The gradual annihilation of electrons and positrons runs down to when T reaches around 1 GK. An $\mathrm{e}^-\mathrm{e}^+$ pair can change to a $\nu_i\bar{\nu}_i$ pair in the reaction listed above, transfering energy from the electrons and positrons to the neutrinos. But $\mathrm{e}^-\mathrm{e}^+$ pairs are usually converted to photons instead.

$$\mathrm{e}^- + \mathrm{e}^+ \quad \leftrightarrow \quad 2\gamma$$

Electromagnetic reactions such as this one occur much more rapidly than the weak reactions between electrons/positrons and neutrinos. So only a small fraction of the electrons and positrons' energy goes to the neutrinos. So small that BBN codes usually ignore it altogether.

Up to now the Texas code and the Thomas et at code have been run with the assumption that there are no reactions between electrons/positrons and neutrinos at any time during the run. In that scenario the neutrinos and the electrons/positrons start out both with Fermi-Dirac distributions and with the same temperature $T = T_\nu$, while the photons start in a Bose-Einstein distribution.

$$f_\gamma(\nu, t) = \frac{1}{\exp(\frac{h\nu}{kT(t)}) - 1}$$

T and T_ν initially obey the rule that $RT =$ a constant. At $T \leq 6$ GK electrons and positrons annilihilate each other transferring all of their energy to the photons. The photons retain their Bose-Einstein distribution, but their heating increases T from the $RT =$ constant rule. In contrast, nothing that would change the evolution of T_ν happens to the neutrinos as they decouple from the other particles, and RT_ν stays constant for the entire run. The entropy density s (Equation (2.23)) of the electromagnetic plasma remains constant. So one can use the high temperature approximation $\rho_{\mathrm{e}^-} = \rho_{\mathrm{e}^+} \approx (7/8)aT^4$ to determine the fractional increase in T due to $\mathrm{e}^-\mathrm{e}^+$ annihilation.

$$\begin{aligned}
s_> &= \frac{R^3}{T}(\rho_{\mathrm{e}^-} + \rho_{\mathrm{e}^+} + \rho_\gamma + p_{\mathrm{e}^+} + p_{\mathrm{e}^-} + p_\gamma) \\
s_> &= \frac{11}{3}a(RT_>)^3 \\
s_< &= \frac{R^3}{T}(\rho_\gamma + p_\gamma) \\
s_< &= \frac{4}{3}a(RT_<)^3
\end{aligned}$$

$$\frac{T}{T_\nu} = (\frac{11}{4})^{1/3}$$

The last equation holds because the entropy density remains constant ($s_> = s_<$).

This author wanted to modify the Texas code so that it would account for the slight coupling of neutrinos and the resulting transfer of energy from the e^-e^+ pairs. To start I had to go back to the energy conservation law $T^{0b}{}_{;b}$, which yields

$$\begin{aligned}
0 &= \dot{\rho}_{total} + 3\frac{\dot{R}}{R}(\rho_{total} + P_{total}) \\
\dot{\rho}_{e+\gamma} &= -4\frac{\dot{R}}{R}\rho_\gamma - 3\frac{\dot{R}}{R}(\rho_e + P_e) - (\dot{\rho}_\nu + 4\frac{\dot{R}}{R}\rho_\nu) \\
\dot{\rho}_{e+\gamma} &= -4\frac{\dot{R}}{R}\rho_\gamma - 3\frac{\dot{R}}{R}(\rho_e + P_e) - \frac{1}{R^4}\frac{d(\rho_\nu R^4)}{dt} \qquad (3.1)
\end{aligned}$$

The last term refers to all three neutrino species and their antiparticles. With no coupling $\rho_{\nu_i} = (7/16)aT_\nu^4$. Then the last term in Equation (3.1) drops out and one gets back Equation (2.10). Equations (3.2) and (3.3) are equations for ρ_{ν_i} written out:

$$\begin{aligned}
\rho_{\nu_i} &= \frac{15}{2\pi^4}a\left(\frac{T_{\nu_o}}{R}\right)^4 \int d\tilde{p}\tilde{p}^3 f_{\nu_i}(\tilde{p}) \qquad (3.2) \\
\dot{\rho}_{\nu_i} &= -4\frac{\dot{R}}{R}\rho_{\nu_i} + \frac{15}{2\pi^4}a\left(\frac{T_{\nu_o}}{R}\right)^4 \int d\tilde{p}\tilde{p}^3 \dot{f}_{\nu_i}(\tilde{p}) \qquad (3.3)
\end{aligned}$$

In Equations (3.2) and (3.3) the momentum variable p is rescaled to $\tilde{p} = (pR)/(kT_{\nu_o})$. At $T = 100$ GK one unit of $\tilde{p}$ is the same as 8.617 MeV of p (the actual value of momentum) and the Fermi-Dirac distribution function $f_{FD}(\tilde{p}) = 1/[\exp(\tilde{p}) + 1]$. Equation (3.3) shows that the time derivatives of the neutrino distribution functions f_{ν_i} are what alter the time evolution of $\rho_{e+\gamma}$.

The Texas code evolves both $\rho_{\mathrm{e}+\gamma}$ and $\ln(R)$, the latter by Equation (2.9). Neutrino heating increases the total ρ_ν, but by the same amount that it decreases $\rho_{\mathrm{e}+\gamma}$. So neutrino heating does not change the time evolution of $\ln(R)$.

Finally recall that the expressions from Chapter (2) for the neutron-proton conversion rates depend on the electron neutrino distribution function f_{ν_e}. These conversion rates have a significant influence over how many neutrons remain by the time of nucleosynthesis, and therefore how much ^{4}He gets made from those neutrons. A change in f_{ν_e} due to neutrino heating can change the conversion rates and then $X_{^4\mathrm{He}}$. Observational $X_{^4\mathrm{He}}$ might one day be measured accurately enough so that the neutrino heating's change in $X_{^4\mathrm{He}}$ can be detectable. The rest of this section will concentrate on $X_{^4\mathrm{He}}$, explaining exactly how neutrino heating can alter this value.

3.2 Previous Approaches

Strictly speaking, to calculate the neutrino heating one has to calculate the change in neutrino distribution functions f_{ν_e}, f_{ν_μ}, and f_{ν_τ} due the scattering and annihilation reactions between them and electrons/positrons, and also of these reactions

$$\begin{array}{ll} \nu_i + \nu_i \leftrightarrow \nu_i + \nu_i & \nu_i + \bar{\nu}_i \leftrightarrow \nu_i + \bar{\nu}_i \\ \nu_i + \nu_j \leftrightarrow \nu_i + \nu_j & \nu_i + \bar{\nu}_j \leftrightarrow \nu_i + \bar{\nu}_j \\ \nu_i + \bar{\nu}_i \leftrightarrow \nu_j + \bar{\nu}_j & \end{array}$$

between the neutrinos themselves (i, j refer to two different neutrino species

). For a two-body reaction 1 + 2 $\leftrightarrow$ 3 + 4 where the particles before and after the reaction are all Fermi-Dirac particles, the evolution of function f_1 of particle 1 is determined by the Boltzmann Transport Equation [38].:

$$
\begin{aligned}
C_L &= C_{coll} \qquad (3.4)\\
C_L &= \frac{\partial f_1(p_1)}{\partial t} - \frac{dR}{dt}\frac{p_1}{R}\frac{\partial f_1(p_1)}{\partial p_1}\\
C_{coll} &= \frac{1}{2E_1}\int \frac{d^3p_2}{2E_2(2\pi)^3}\frac{d^3p_3}{2E_3(2\pi)^3}\frac{d^3p_4}{2E_4(2\pi)^3}\Lambda(f_1,f_2,f_3,f_4)\times\\
&\quad S|M|^2_{12\rightarrow 34}\delta^4(p_1+p_2-p_3-p_4)(2\pi)^4\\
\Lambda(f_1,f_2,f_3,f_4) &= \{[1-f_1(p_1)][1-f_2(p_2)]f_3(p_3)f_4(p_4)\\
&\quad -f_1(p_1)f_2(p_2)[1-f_3(p_3)][1-f_4(p_4)]\}
\end{aligned}
$$

Equation (3.4) corresponds to the case of a homogeneous cosmology. C_L, the Liouville Operator, is the covariant and relativistic form of the total time derivative of f_1. C_{coll}, the Collision Operator, accounts for the change in f_1 due to the 1 + 2 $\leftrightarrow$ 3 + 4 reaction. In an analogy to Equation (2.4) for the isotope abundances $Y(i)$ the term proportional to $f_1 f_2$ corresponds to the destruction of particle 1 due to the forward direction of this reaction while the term proportional to $f_3 f_4$ corresponds to the production of particle 1 due to the reverse direction. $S|M|^2$ consists of the matrix elements for the reactions. Tables (3.1a) and (3.2a) list the $S|M|^2$ terms for each reaction. The second term in C_L accounts for the expansion of the universe. But one can get rid of this term simply by rescaling all the p_i to $\tilde{p}_i = (p_i R)/(kT_{\nu_o})$, as was done for Equation (3.2).

$$
C_L = \frac{\partial f_1(\tilde{p}_1)}{\partial t}
$$

$$
\begin{aligned}
C_{coll} &= \frac{1}{2E_1}\left(\frac{kT_N}{R}\right)^5 \int \frac{d^3\tilde{p}_2}{(2\pi)^3 2E_2}\int \frac{d^3\tilde{p}_3}{(2\pi)^3 2E_3}\int \frac{d^3\tilde{p}_4}{(2\pi)^3 2E_4} S|M|^2 \\
&\quad (2\pi)^4\delta^4(\tilde{p}_1+\tilde{p}_2-\tilde{p}_3-\tilde{p}_4)\Lambda(f_1,f_2,f_3,f_4)
\end{aligned}
$$

For the rest of the chapter the tilde's are dropped, and p in any equation is the rescaled p unless specified otherwise.

The Boltzmann Transport Equation...is very complicated to solve. So early articles on neutrino heating (HH:1989 [39]; RM, 1991 [40]; RM, 1984 [21]) try to avoid the Boltzmann equation altogether in calculating the effect. The Texas code still had the method of calculating the heating effect described in detail in (RM, 1984) [21] when this author started working on it. Heating increases the distribution function's value. In (RM, 1984) Rothman and Matzner assume that heating increases $f_{\nu_i}(p_{\nu_i})$ for each species i by the same proportional amount regardless of the value of p_{ν_i}. They explain how based on that assumption they could derive their equations for the time derivatives of the expressions $\rho_{\nu_i}R^4$ and $n_{\nu_i}R^3$, both of which were constant without the heating effect. For instance for the electron neutrinos:

$$
\begin{aligned}
\frac{d}{dt}(n_{\nu_e}R^3) &= -\left(\frac{n_{\nu_e}R^3}{t(\nu_e\bar{\nu}_e\to e^-e^+)}+\frac{n_{\nu_e}R^3}{t(\nu_e\bar{\nu}_e\to\nu_\mu\bar{\nu}_\mu)}+\frac{n_{\nu_e}R^3}{t(\nu_e\bar{\nu}_e\to\nu_\tau\bar{\nu}_\tau)}\right) \\
&\quad +\frac{n_{\nu_\mu}R^3}{t(\nu_\mu\bar{\nu}_\mu\to\nu_e\bar{\nu}_e)}+\frac{n_{\nu_\tau}R^3}{t(\nu_\tau\bar{\nu}_\tau\to\nu_e\bar{\nu}_e)}+\frac{n_e R^3}{t(e^-e^+\to\nu_e\bar{\nu}_e)} \\
\frac{d}{dt}(\rho_{\nu_e}R^4) &= -\frac{\rho_{\nu_e}R^4}{t(\nu_e\to)}+\frac{\rho_{\nu_e}R^4}{t(\nu_e\to\nu_e)}+\frac{\rho_{\nu_\mu}R^4}{t(\nu_\mu\to\nu_e)}+\frac{\rho_{\nu_\tau}R^4}{t(\nu_\tau\to\nu_e)} \\
&\quad +\frac{\rho_e R^4}{t(e\to\nu_e)}
\end{aligned}
$$

(RM, 1984) simply use an average collision time to account for each collision's influence. For instance $t(\nu_e\to)$ is the average time of all collisions with ν_e as

Process	$S\|M\|^2$
$\nu_\mathrm{e} + \nu_\mathrm{e} \to \nu_\mathrm{e} + \nu_\mathrm{e}$	$32G_F^2(p_1 \cdot p_2)(p_3 \cdot p_4)$
$\nu_\mathrm{e} + \nu_i \to \nu_\mathrm{e} + \nu_i$	$32G_F^2(p_1 \cdot p_2)(p_3 \cdot p_4)$
$\nu_\mathrm{e} + \bar{\nu}_i \to \nu_\mathrm{e} + \bar{\nu}_i$	$32G_F^2(p_1 \cdot p_4)(p_2 \cdot p_3)$
$\nu_\mathrm{e} + \bar{\nu}_\mathrm{e} \to \nu_i + \bar{\nu}_i$	$32G_F^2(p_1 \cdot p_4)(p_2 \cdot p_3)$
$\nu_\mathrm{e} + \bar{\nu}_\mathrm{e} \to \nu_e + \bar{\nu}_e$	$128G_F^2(p_1 \cdot p_4)(p_2 \cdot p_3)$
$\nu_\mathrm{e} + \mathrm{e}^- \to \nu_\mathrm{e} + \mathrm{e}^-$	$32G_F^2[(C_A + C_V)^2(p_1 \cdot p_2)(p_3 \cdot p_4)$
	$+(C_A - C_V)^2(p_1 \cdot p_4)(p_2 \cdot p_3)$
	$-(C_V^2 - C_A^2)m_\mathrm{e}^2(p_1 \cdot p_3)]$
$\nu_\mathrm{e} + \mathrm{e}^+ \to \nu_\mathrm{e} + \mathrm{e}^+$	$32G_F^2[(C_A - C_V)^2(p_1 \cdot p_2)(p_3 \cdot p_4)$
	$+(C_A + C_V)^2(p_1 \cdot p_4)(p_2 \cdot p_3)$
	$-(C_V^2 - C_A^2)m_\mathrm{e}^2(p_1 \cdot p_3)]$
$\nu_\mathrm{e} + \bar{\nu}_\mathrm{e} \to \mathrm{e}^- + \mathrm{e}^+$	$32G_F^2[(C_A + C_V)^2(p_1 \cdot p_4)(p_2 \cdot p_3)$
	$+(C_A - C_V)^2(p_1 \cdot p_3)(p_2 \cdot p_4)$
	$+(C_V^2 - C_A^2)m_\mathrm{e}^2(p_1 \cdot p_2)]$

Process	$S\|M\|^2$
$\nu_i + \nu_i \to \nu_i + \nu_i$	$32G_F^2(p_1 \cdot p_2)(p_3 \cdot p_4)$
$\nu_i + \nu_j \to \nu_i + \nu_j$	$32G_F^2(p_1 \cdot p_2)(p_3 \cdot p_4)$
$\nu_i + \nu_\mathrm{e} \to \nu_i + \nu_\mathrm{e}$	$32G_F^2(p_1 \cdot p_2)(p_3 \cdot p_4)$
$\nu_i + \bar{\nu}_j \to \nu_i + \bar{\nu}_j$	$32G_F^2(p_1 \cdot p_4)(p_2 \cdot p_3)$
$\nu_i + \bar{\nu}_\mathrm{e} \to \nu_i + \bar{\nu}_\mathrm{e}$	$32G_F^2(p_1 \cdot p_4)(p_2 \cdot p_3)$
$\nu_i + \bar{\nu}_i \to \nu_j + \bar{\nu}_j$	$32G_F^2(p_1 \cdot p_4)(p_2 \cdot p_3)$
$\nu_i + \bar{\nu}_i \to \nu_\mathrm{e} + \bar{\nu}_\mathrm{e}$	$32G_F^2(p_1 \cdot p_4)(p_2 \cdot p_3)$
$\nu_i + \bar{\nu}_i \to \nu_i + \bar{\nu}_i$	$128G_F^2(p_1 \cdot p_4)(p_2 \cdot p_3)$
$\nu_i + \mathrm{e}^- \to \nu_i + \mathrm{e}^-$	$32G_F^2\{(C_A + C_V - 2)^2(p_1 \cdot p_2)(p_3 \cdot p_4)$
	$+(C_A - C_V)^2(p_1 \cdot p_4)(p_2 \cdot p_3)$
	$-[(C_V - 1)^2 - (C_A - 1)^2]m_\mathrm{e}^2(p_1 \cdot p_3)\}$
$\nu_i + \mathrm{e}^+ \to \nu_i + \mathrm{e}^+$	$32G_F^2\{(C_A - C_V)^2(p_1 \cdot p_2)(p_3 \cdot p_4)$
	$+(C_A + C_V - 2)^2(p_1 \cdot p_4)(p_2 \cdot p_3)$
	$-[(C_V - 1)^2 - (C_A - 1)^2]m_\mathrm{e}^2(p_1 \cdot p_3)\}$
$\nu_i + \bar{\nu}_i \to \mathrm{e}^- + \mathrm{e}^+$	$32G_F^2\{(C_A + C_V - 2)^2(p_1 \cdot p_4)(p_2 \cdot p_3)$
	$+(C_A - C_V)^2(p_1 \cdot p_3)(p_2 \cdot p_4)$
	$+[(C_V - 1)^2 - (C_A - 1)^2]m_\mathrm{e}^2(p_1 \cdot p_2)\}$

Table 3.1: The matrix elements corresponding to each weak reaction in the Boltzmann Transport Equation. (3.1a) is for ν_e as particle # 1 in the equation, and (3.1b) is for $\nu_{\mu,\tau}$ as particle # 1.

an incoming particle, $t(\nu_\mu \to \nu_e)$ is the time for all collisions with ν_μ as an incoming particle and ν_e as an outgoing particle, and so forth. The Texas code can evolve $\rho_{\nu_i} R^4$ and $n_{\nu_i} R^3$ using the second-order Runge-Kutta method, and in the code's conversion rate equations f_{ν_e} is multiplied by a factor that accounts for the increase due to heating. The increase in f_{ν_i} independent of the momentum value characterizes the "One Bin" approach these articles ([39], [40], [21]) use to solve for the heating effect.

In their PRD article (DT, 1992) [30] Dodelson and Turner try to solve for f_{ν_i} itself. They select 60 values of momentum p and solve the Boltzmann equation for $f_{\nu_e}(p)$ and $f_{\nu_\mu}(p) = f_{\nu_\tau}(p)$ at all those 60 values. So they have a "MultiBin" method of calculating the heating effect using 60 bins. To make the Boltzmann equation easier to solve Dodelson and Turner set the electron mass m_e to zero in the matrix elements, and use Maxwell-Boltzmann statistics in the phase space factor.

$$\Lambda(f_1, f_2, f_3, f_4) = f_3(p_3) f_4(p_4) - f_1(p_1) f_2(p_2)$$

Dodelson and Turner look at the first-order pertubations of f_{ν_i} from the Fermi-Dirac distribution f_{FD} and the fractional difference $\delta(t)$ between the electromagnetic plasma's T and T_ν from the case of no heating.

$$\begin{aligned} f_{\nu_i}(p) &\approx f_{\mathrm{FD}}(p) + \Delta_{\nu_i}(p,t) \\ \delta(t) &= \frac{T}{T_\nu} - 1 \end{aligned}$$

They derive expressions for $\Delta_{\nu_i}(p,t)$ and $\delta(t)$ from the Boltzmann equation and evolve them through second-order Runge-Kutta. (DT, 1992) shows how the MultiBin method reveals that neutrino heating is momentum dependent, and their followup article cowritten with Brian Fields [31] gives their results on how the heating effect changes $X_{^4\mathrm{He}}$.

For their 1995 PRD article [32] Hannestad and Madsen used a MultiBin model without the appoximations used by Fields, Dodelson and Turner. Their version of the Boltzmann equation uses Fermi-Dirac statistics and has a nonzero value for m_{e}, and they solve for and evolve $f_{\nu_{\mathrm{e}}}$ and $f_{\nu_\mu} = f_{\nu_\tau}$ rather than the first-order pertubations of the distribution functions. They also show that the Boltzmann equation can in fact be solved analytically down to two integrand variables. The means of solving for the heating effect used in this dissertation is modelled after Hannestad and Madsen's method.

3.3 Scheme to Solve the Boltzmann Equation

For a reaction $1 + 2 \leftrightarrow 3 + 4$ one can solve the Boltzmann equation down to a double integral of the momenta p_2 and p_3. For all the reactions C_{coll} will have the form

$$\begin{aligned} C_{coll} &= \int dp_2 \int dp_3 F(p_1, p_2, p_3)\{[1 - f_1(p_1)][1 - f_2(p_2)]f_3(p_3)f_4(p_4) \\ &\quad - f_1(p_1)f_2(p_2)[1 - f_3(p_3)][1 - f_4(p_4)]\} \end{aligned} \tag{3.5}$$

The boundaries over which p_2 and p_3 are integrated depend on the specific reaction. p_4 can be written as a function of p_1, p_2, and p_3, and m_{e} for reactions involving electrons and positrons. $F(p_1, p_2, p_3)$ is a complicated polynomial of the momenta that might also include terms dependent on m_{e}. The Appendix at the end of this chapter describes in detail how to derive C_{coll} for every reaction in Tables (3.1a) and (3.1b).

The two remaining integrals in C_{coll} have to be rewritten as approximating sums. Also f_{ν_e} and f_{ν_μ} are now unknown except for when the code starts at $T = 100$ GK. But one can define a finite grid of momentum values $p_i(j)$ and use the Boltzmann Transport Equation to evolve $f_{\nu_e}[p_i(j)]$ and $f_{\nu_\mu}[p_i(j)]$ at every point j. For this disseratation the author picked 100 evenly spaced values of $p(j)$ ranging from 0.25 to 25.0.

For the reactions where all particles were neutrinos this author used the extended trapezoidal rule write the integrals in C_{coll} as sums. For instance for the reaction $\nu_\mathrm{e} + \nu_\mu \leftrightarrow \nu_\mathrm{e} + \nu_\mu$

$$\begin{aligned} C_{coll} \;=\; & \sum_{j_2=0}^{100} \sum_{j_3=0}^{j_1+j_2} (\Delta p)^2 C_1 C_2 F(p_1, p_2, p_3) \\ & \{[1 - f_{\nu_e}(p_1)][1 - f_{\nu_\mu}(p_2)] f_{\nu_e}(p_3) f_{\nu_\mu}(p_1 + p_2 - p_3) \\ & - f_{\nu_e}(p_1) f_{\nu_\mu}(p_2)[1 - f_{\nu_e}(p_3)][1 - f_{\nu_\mu}(p_1 + p_2 - p_3)]\} \qquad (3.6) \end{aligned}$$

where $p_i = p(j_i)$. The coefficients C_1 and C_2 equal 0.5 at the minimum and maximum values of p_2 and p_3 and 1.0 everwhere else, and $\Delta p = 0.25$. The grid is defined such that $p_4 = p_1 + p_2 - p_3$ always falls on a grid point. The phase space factor is a nonlinear function of f_{ν_e} and f_{ν_μ}. When T is at its highest values the phase space factor is a relatively small difference between two large numbers. So Equation (3.6) is analogous to Equation (2.4), the equation for the time derivative of the isotope abundances. One can treat the combined 200 values of $f_{\nu_e}[p_i(j)]$ and $f_{\nu_\mu}[p_i(j)]$ in the same way as one handles the 68 abundances $Y(i)$. One solves the Boltzmann Transport Equation by linearizing Equation (3.6) the same way one linearizes (2.4) to get Equations (2.19) and (2.25) from the Thomas et al code.

For the first Runge-Kutta step define the functions $f_{\nu_{e(\alpha)}}(p(j), t_n)$ and $f_{\nu_{\mu(\alpha)}}(p(j), t_n)$ as functions nearly equal to $f_{\nu_e}(p(j), t_n)$ and $f_{\nu_\mu}(p(j), t_n)$ that have to solve the following equation.

$$
\begin{aligned}
C_{coll} &= \frac{f_{\nu_{e(\alpha)}}(p_1, t_n) - f_{\nu_e}(p_1, t_{n-1})}{\Delta t_{n-1}} \qquad (3.7)\\
C_{coll} &= \sum_{j_2=0}^{100} \sum_{j_3=0}^{j_1+j_2} (\Delta p)^2 C_1 C_2 F(p_1, p_2, p_3) \\
&\Big\{\frac{1}{2}[f_{\nu_{e(\alpha)}}(p_3, t_n) f_{\nu_\mu}(p_4, t_n) + f_{\nu_e}(p_3, t_n) f_{\nu_{\mu(\alpha)}}(p_4, t_n)] \\
&-\frac{1}{2}[f_{\nu_{e(\alpha)}}(p_1, t_n) f_{\nu_\mu}(p_2, t_n) + f_{\nu_e}(p_1, t_n) f_{\nu_{\mu(\alpha)}}(p_2, t_n)] \\
&-\frac{1}{3}[f_{\nu_{e(\alpha)}}(p_1, t_n) f_{\nu_e}(p_3, t_n) f_{\nu_\mu}(p_4, t_n) \\
&+f_{\nu_e}(p_1, t_n) f_{\nu_{e(\alpha)}}(p_3, t_n) f_{\nu_\mu}(p_4, t_n) \\
&+f_{\nu_e}(p_1, t_n) f_{\nu_e}(p_3, t_n) f_{\nu_{\mu(\alpha)}}(p_4, t_n)] \\
&-\frac{1}{3}[f_{\nu_{\mu(\alpha)}}(p_2, t_n) f_{\nu_e}(p_3, t_n) f_{\nu_\mu}(p_4, t_n) \\
&+f_{\nu_\mu}(p_2, t_n) f_{\nu_{e(\alpha)}}(p_3, t_n) f_{\nu_\mu}(p_4, t_n) \\
&+f_{\nu_\mu}(p_2, t_n) f_{\nu_e}(p_3, t_n) f_{\nu_{\mu(\alpha)}}(p_4, t_n)] \\
&+\frac{1}{3}[f_{\nu_{e(\alpha)}}(p_1, t_n) f_{\nu_\mu}(p_2, t_n) f_{\nu_e}(p_3, t_n) \\
&+f_{\nu_e}(p_1, t_n) f_{\nu_{\mu(\alpha)}}(p_2, t_n) f_{\nu_e}(p_3, t_n) \\
&+f_{\nu_e}(p_1, t_n) f_{\nu_\mu}(p_2, t_n) f_{\nu_{e(\alpha)}}(p_3, t_n)] \\
&+\frac{1}{3}[f_{\nu_{e(\alpha)}}(p_1, t_n) f_{\nu_\mu}(p_2, t_n) f_{\nu_\mu}(p_4, t_n) \\
&+f_{\nu_e}(p_1, t_n) f_{\nu_{\mu(\alpha)}}(p_2, t_n) f_{\nu_\mu}(p_4, t_n) \\
&+f_{\nu_e}(p_1, t_n) f_{\nu_\mu}(p_2, t_n) f_{\nu_{\mu(\alpha)}}(p_4, t_n)]\Big\}
\end{aligned}
$$

This equation is analogous to Equation (2.19). All these terms come from writing out the phase space factor explicitly and then linearizing it with respect to $f_{\nu_e(\alpha)}(p(j), t_n)$ and $f_{\nu_\mu(\alpha)}(p(j), t_n)$. (Only the four terms with a coefficient (1/2) in front of them remain if one uses Maxwell-Boltzmann statistics instead of Fermi-Dirac.) One then just rearrange the equation into a matrix equation for $f_{\nu_e(\alpha)}$ and $f_{\nu_\mu(\alpha)}$, solve for $f_{\nu_e(\alpha)}$ and $f_{\nu_\mu(\alpha)}$, and plug it back into the above equation to get the first R-K derivative $df_{\nu_e(p_1)}/dt$. And for the second R-K derivative one defines an $f_{\nu_e(\beta)}(p(j), t_n)$ and $f_{\nu_\mu(\beta)}(p(j), t_n)$ that solves an equation analogous to Equation (2.25).

Electrons and positrons will always have Fermi-Dirac distributions. So $f_e(p, t)$ is known for all momenta and all time. For the reactions involving electrons and positrons then one can use summations other than the trapezoidal role for integrations over electron momenta, and the linearized phase space factor is not as complicated as the factor for reactions that have only neutrinos.

3.4 Results

The results discussed in the rest of this chapter are all for baryon-to-photon ratio $\eta_{10} = 3.0$. Left on its own to determine the timestep values the Texas code takes 1781 steps to run for this value of η_{10} for the case of full neutrino heating, with all the reactions between neutrinos, electrons and positrons working. This author does a neutrino heating run and save the timestep values, and then feeds the 1781 timestep values back into the code for a run with no neutrino heating. The sections of the code used to do convergence tests of the mass fractions enable one to feed values of Δt directly into the code. This way the Texas code can give abundances, reaction rates, and energy densities for both with neutrino heating and without heating at set values of time t, and one can compare the sets of data directly with each other. The larger number of timesteps changes the final mass fractions for the case of no heating from the values listed in Table (2.8). Table (3.4) lists the final mass fractions when the Texas code is run with 1781 timesteps and no heating. $X_{^4\mathrm{He}}$ goes up from 0.239020 to 0.239071, one order of magnitude less than the expected change due to the heating effect, and the other mass fractions tend to increase or decrease by an amount 10^{-4} times their magnitudes.

The phase space factor will always equal zero if all four distribution functions are Fermi-Dirac functions with the same temperature. On their own the reactions that involve only neutrinos cannot change the distribution functions. Runs with only the neutrino-only reactions working confirm that $f_{\nu_\mathrm{e}}(p)$ and $f_{\nu_\mu}(p)$ do not change in such a run. And the reactions involving electrons/positrons could not change $f_{\nu_\mathrm{e}}(p)$ and $f_{\nu_\mu}(p)$ either if electrons and positrons maintain the same temperature as the neutrinos. But the electromagnetic plasma's temperature instead increases because $\mathrm{e}^-\mathrm{e}^+$ annihilation frees up the pairs' rest mass energies and transfers the energy to massless photons. This energy gets transferred to the neutrinos as well via the annihilation reaction $\mathrm{e}^- + \mathrm{e}^+ \rightarrow \nu_\mathrm{e} + \bar{\nu}_\mathrm{e}$ and the scattering reactions $\nu_\mathrm{e} + \mathrm{e}^\pm \rightarrow \nu_\mathrm{e} + \mathrm{e}^\pm$. For $T =$ from 20 GK down to 1 GK $f_{\nu_\mathrm{e}}(p)$ and $f_{\nu_\mu}(p)$ increase significantly.

Figure (3.1a) shows the fractional increase in $f_{\nu_\mathrm{e}}(p)$ for p with a range from 0.0 to 25.0, starting from its Fermi-Dirac distribution. At high enough temperatures neutrinos of rescaled momentum p are energetic enough to create $\mathrm{e}^-\mathrm{e}^+$ pairs as rapidly as $\mathrm{e}^-\mathrm{e}^+$ pairs create them. But as the universe expands rescaled p corresponds to a lower and lower value of physical p. At a certain temperature neutrinos of momentum p no longer have the energy to maintain the reactions between them and electrons/positrons, and they decouple from

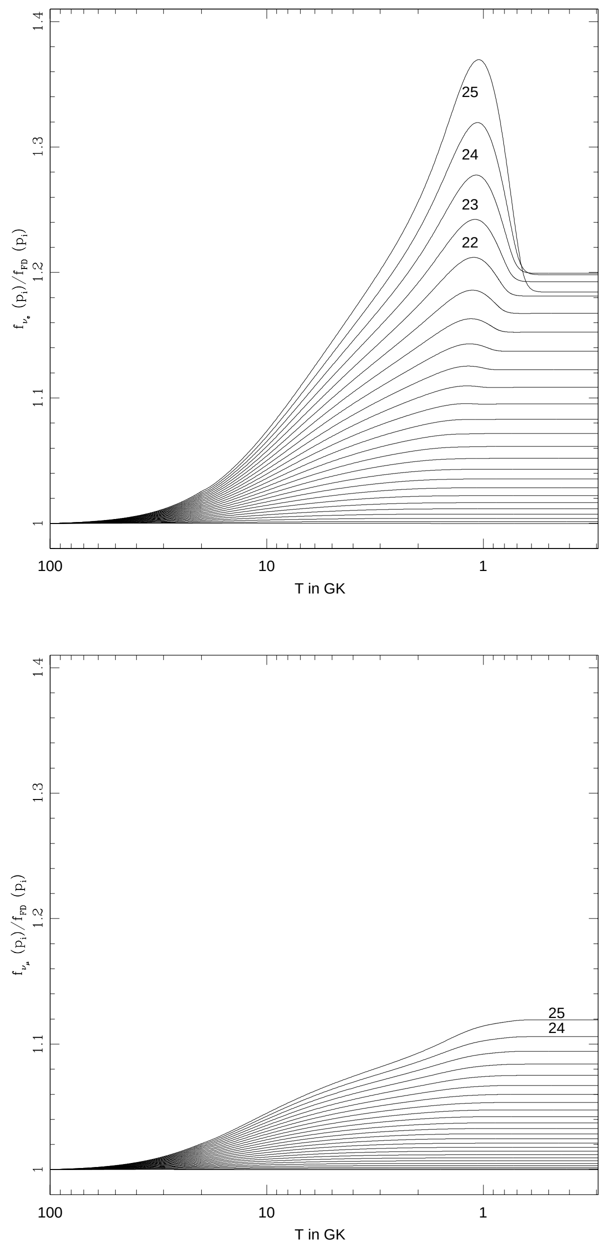

Figure 3.1: The increase in the distribution functions f_{ν_e} (3.1a) and f_{ν_μ} (3.1b) due to neutrino heating. f_{ν_i} is normalized to its Fermi-Dirac value f_{FD}.

e^- and e^+. Each graph in Figure (3.1a) has a point where $f_{\nu_e}(p)$ levels off to its final value. The more energetic the neutrinos the longer they can stay coupled with the electrons/positrons. So with increasing p $f_{\nu_e}(p)$ increases more rapidly and the value of T in each graph when $f_{\nu_e}(p)$ levels off decreases. Figure (3.1a) shows how the actual evolution of $f_{\nu_e}(p)$ differs considerably from the assumption that $f_{\nu_e}(p)$ increases equally for all p that the One-Bin models use. The electron neutrinos with the highest p's stay coupled with the electrons/positrons all the way down to $T = 1$ GK, when e^-e^+ pairs have been almost completely depleted. But the neutrino-only reactions still run, redistributing the energy of the high momentum electron neutrinos down to the low momentum electron neutrinos and the muon/tau neutrinos. Also, the highest energy electron neutrinos can be energetic enough to annihilate and produce new e^-e^+ pairs. So the graphs for the high momentum $f_{\nu_e}(p)$ decrease before they reach their final values. In this run they decrease so much that $f_{\nu_e}(25)/f_{\mathrm{FD}}(25)$ ends up lower than $f_{\nu_e}(23)/f_{\mathrm{FD}}(23)$. But this result comes from the limitations of the grid. When the code was run with only a 50 point grid $f_{\nu_e}(25)/f_{\mathrm{FD}}(25)$ dropped considerably more, as did $f_{\nu_e}(p)/f_{\mathrm{FD}}(p)$ for p near 25. The larger grid has more high energy bins, and so less energy from each bin needs to be depleted to achieve the same energy transfer. Also in reality there would be electron neutrinos of higher energy that would be able to track electrons/positrons even more closely, and transfering energy to the bins that are the highest in my grid. This author concludes that the decrease in the graphs is a real phenomenom but the final values of $f_{\nu_e}(p)/f_{\mathrm{FD}}(p)$ would always increase with increasing p.

Figure (3.1b) shows $f_{\nu_\mu}(p)$ for the muon neutrinos. Reactions between muon neutrinos and electrons/positrons involve only neutral current interactions, vs. the neutral and charged current reactions that electron neutrinos can undergo with them. This is reflected in the replacement of C_A and C_V with $C_A - 1$ and $C_V - 1$ in the matrix elements for the muon neutrino reactions. So the increases of $f_{\nu_\mu}(p)/f_{\rm FD}(p)$ come out considerably smaller than for $f_{\nu_{\rm e}}(p)/f_{\rm FD}(p)$. At $T = 1$ GK the muon neutrinos receive energy from the higher temperature electron neutrinos. $f_{\nu_\mu}(p)/f_{\rm FD}(p)$ for the highest p then keeps increasing up to $T = 0.7$ GK when $f_{\nu_\mu}(p)/f_{\rm FD}(p)$ starts to asymptote. That's about the same temperature as when the highest momentum $f_{\nu_{\rm e}}(p)/f_{FD}(p)$ reach their final values. The code is written such that $f_{\nu_\tau}(p) = f_{\nu_\mu}(p)$

Figures (3.2) show what the reaction rates exactly look like for the case when Particle # 1 in the reactions is an electron neutrino with momentum $p = 25.0$. For each reaction the rate of one direction is subtracted from the rate of the other, and the graphs in these figures show the net difference between the directions. The graphs are labelled with the reactions in the direction that prevails. Figure (3.2a) shows the rates for reactions that have an electron neutrino with $p = 25.0$ as an outgoing particle, and Figure (3.2b) show rates with an electron neutrinos with $p = 25.0$ as an incoming particle. As expected the reactions that produce neutrinos with this momentum involve electrons and positrons, while the reactions with lower energy electron neutrinos and muon/tau neutrinos deplete them.

After the Texas code carries out the first Runge-Kutta step for both the abundances $Y(i)$ and the neutrino distribution functions $f_{\nu_{\rm e}}[p(i)]$ and $f_{\nu_\mu}[p(i)]$ (Equation (3.7)) the code calculates a new timestep difference Δt_n not only from $Y(i)$, $\ln R$ and $\rho_{{\rm e}+\gamma}$ but from the distribution functions as well.

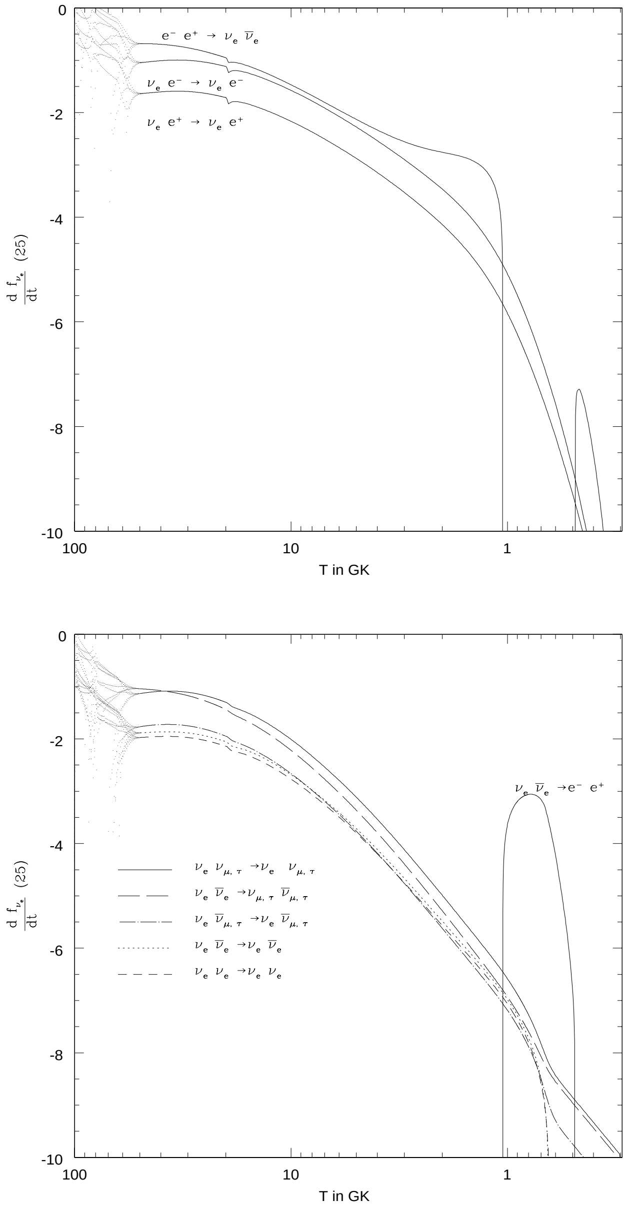

Figure 3.2: The rates of reactions that change the value of f_{ν_e} for a ν_e with momentum $p = 25$. (3.2a) shows rates that have this ν_e as an outgoing particle, and (3.2b) shows rates with this ν_e as an incoming particle. The graphs become stable about when T reaches 50 GK.

$$\Delta t_n \quad = \quad (dk_f)(dk)\min\left[\frac{f_{\nu_e}[p(i),t_n]}{\frac{df_{\nu_e}}{dt}[p(i)]}, \frac{f_{\nu_\mu}[p(i),t_n]}{\frac{df_{\nu_\mu}}{dt}[p(i)]}\right]$$

The Texas code still has a problem with carrying out the Runge-Kutta method in solving for $f_{\nu_e}[p(i)]$ and $f_{\nu_\mu}[p(i)]$ stably at the highest temperatures. When the phase space factor is a small difference between two large numbers the results for (df_{ν_e}/dt) and (df_{ν_μ}/dt) oscillate considerably between positive and negative values. Thus the graphs in Figures (3.2) start out as disconnected points. To prevent this oscillation from affecting $f_{\nu_e}[p(i)]$ and $f_{\nu_\mu}[p(i)]$ this author has to put in an extra factor $dk_f = 0.001$. This dk_f reduces the timestep differences so much as that the distribution functions do not increase considerably for $T > 50$ GK. At $T = 50$ GK the oscillation dies down, and the graphs in (3.2) start behaving smoothly. By $T = 20$ GK (df_{ν_e}/dt) and (df_{ν_μ}/dt) have behaved smoothly for quite sometime, and are large enough so that quantities other than the distribution functions determine the timestep difference. So dk_f can safely increase from 0.001 to 0.01. That change in dk_f accounts for the small nicks in the graphs at $T = 20$ GK.

At $T =$ from 50 GK to 20 GK the neutrino-only reactions in Figure (3.2b) are comparable in magnitude to the reactions involving electrons and positrons in Figure (3.2a). The neutrino-only reactions can thermalize the heat transferred via the electron/positron reactions and so $f_{\nu_e}(25)$ as well as the other graphs in Figures (3.1) don't increase that much. But the temperature difference between e^-e^+ pairs and neutrinos eventually becomes great enough that the reaction rates in Figure (3.2a) have considerably larger magnitudes than the rates in Figure (3.2b) by the time when $T = 10$ GK. The distribution functions increase the most when $T = 10$ GK down to 1 GK. e^-e^+ annihilation yields a larger increase of $f_{\nu_e}(25)$ then the reactions where the electron neutrino only scatters off of an electron or positron, and the neutrino will get energy from an electron more efficiently than from a positron. Figure (3.2b) shows that electron neutrinos with $p = 25$ lose more energy through reactions with muon neutrinos and τ neutrinos than with electron neutrinos of lesser energy. But Figure (3.2b) also shows that at $T = 1$ GK the direction $\nu_e + \bar{\nu}_e \rightarrow$ $e^- + e^+$ now prevails. e^-e^+ pairs have been depleted while electron neutrinos with $p = 25.0$ are still energetic enough to create e^-e^+ pairs. So $\nu_e\bar{\nu}_e$ annihilation becomes the dominant reaction, and the neutrino-only reactions are still running. These graphs explain why the highest graphs in Figure (3.1a) start decreasing, and the graphs in Figure (3.1b) have a slight dent meaning that $f_{\nu_\mu}[p(i)]$ is increasing more quickly.

Figure (3.3) shows the fractional increase of ρ_{ν_e} and ρ_{ν_μ} due to neutrino heating. ρ_{ν_e} increases by 0.935 % while ρ_{ν_μ} increases by 0.384 %. ρ_{ν_e} reaches its asymptotic value at $T =$ slightly under 2 GK. Graphs in Figure (3.1a) for p up to 16 reach their final values at around 2 GK or higher. $f_{\nu_e}(p)$ for higher p must then make too small a contribution to Equation (3.2) to significantly change ρ_{ν_e}. So the grid dependent decrease of the final values of high momentum $f_{\nu_e}(p)/f_{\rm FD}(p)$ has no significant influence in the final value of physical quantities.

Figure (3.3) also shows the increase of ρ_{ν_e} and ρ_{ν_μ} when there is no electron or positron scattering, when there is no electron/positron annihilation, and when there are no neutrino-only reactions. Figure (3.4a) shows $f_{\nu_e}[p(i)]$ for the case without e^- and e^+ scattering. The graphs are smaller here than in Figure (3.1a). But ρ_{ν_e} and ρ_{ν_μ} don't decrease very much as a result. Only down to 0.863 % and 0.353 % respectively. The highest graphs decrease in

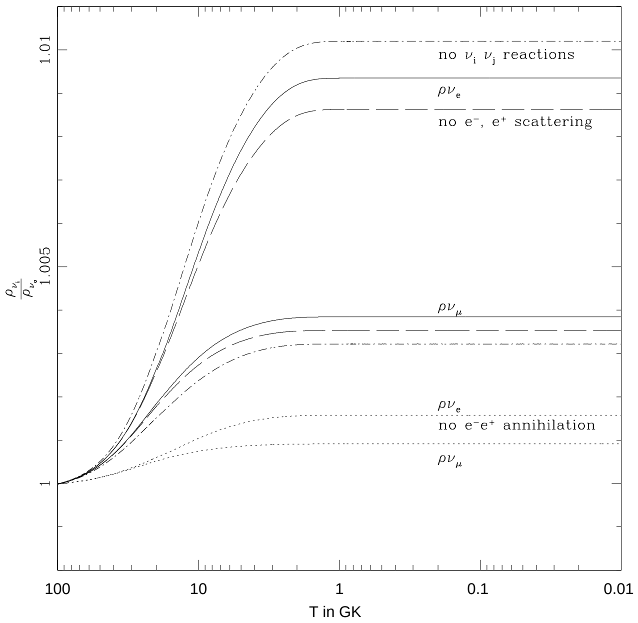

Figure 3.3: The increase of ρ_{ν_e} and ρ_{ν_μ} due to neutrino heating. Both ρ_ν's are normalized to their Fermi-Dirac values ρ_{ν_o}. The results when e^-e^+ annihilation, e^-, e^+ scattering, or $\nu_i\nu_j$ reactions are also shown.

Figure (3.4a) as well as Figure (3.1a), and they decrease considerably more because the scattering reactions aren't there to add energy to the electron neutrinos. Figure (3.4b) shows $f_{\nu_e}[p(i)]$ for the case of e^- and e^+ scattering only. As the scattering reaction rates decrease steadily without changing sign the graphs in Figure (3.4b) simply increase and asymptote. But the scattering reactions transfer energy to the neutrinos less efficiently than e^-e^+ annihilation. Scattering results in only a small increase in ρ_{ν_e} and ρ_{ν_μ}, 0.158 % and 0.091 % respectively. Figure (3.3) also shows that the reactions between electron neutrinos and muon/tau neutrinos are a significant energy source for the muon and tau neutrinos. With those reactions taken away, electron neutrinos retain more energy and ρ_{ν_e} has a final value 1.02 % higher than with

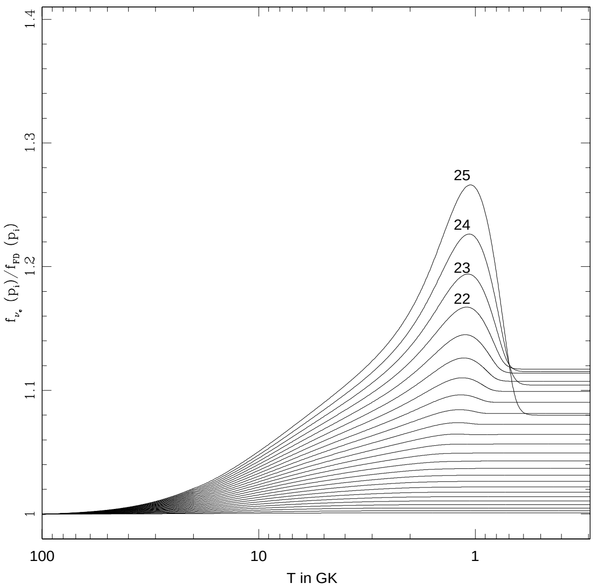

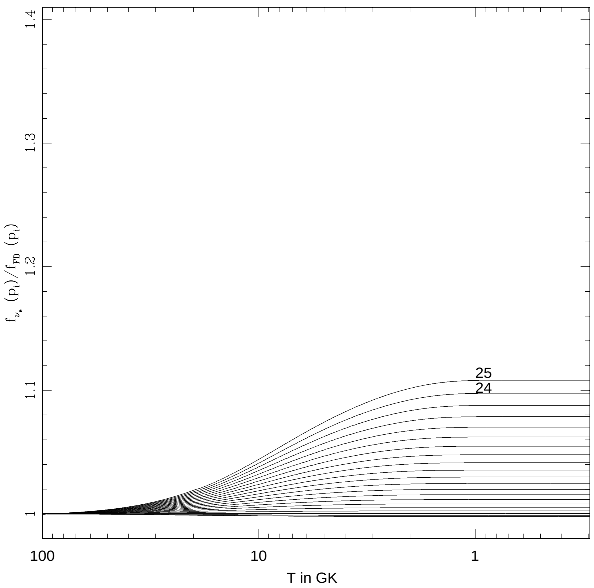

Figure 3.4: The increase of f_{ν_e} when e^-, e^+ scattering is left out (3.4a), when e^-e^+ annihiliation is left out (3.4b), and when $\nu_i\nu_j$ reactions are left out (3.4c). When e^-e^+ annihiliation is left out f_{ν_e} never decreases.

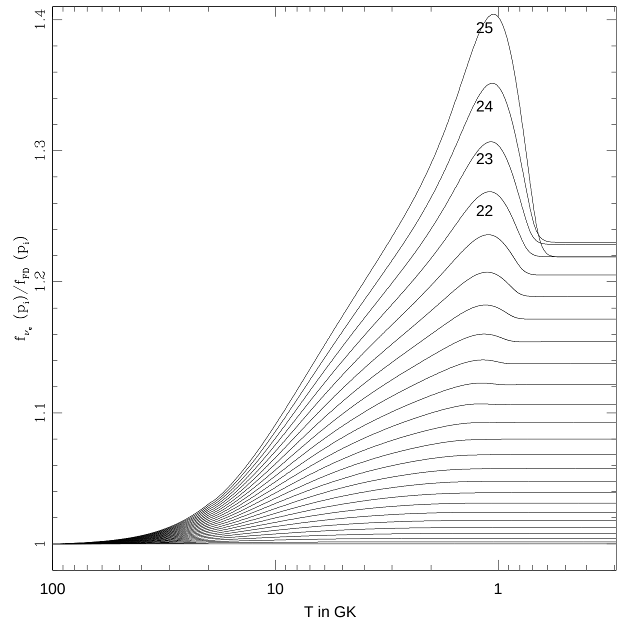

no heating, while muon neutrinos aren't heated as much as the case with the neutrino-only reactions, and ρ_{ν_μ} has only a 0.322 % increase. The graphs for the neutrino-only case diverge from the cases of all reactions present and all but e^- and e^+ scattering present right from the start, illustrating how significant the neutrino-only reactions are at the highest temperatures. Figure (3.4c) shows $f_{\nu_e}[p(i)]$ for the case without neutrino-only reactions, where the graphs are larger than in Figure (3.1a) as indicated by Figure (3.3).

The following sets of graphs show how neutrino heating changes the neutron proton conversion rates, the mass fraction X_n of free neutrons and $X_{^4\mathrm{He}}$ of ^{4}He. Table (3.2) describes the conditions of the code for each set of data. Note though that in most of these different situations the electromagnetic plasma temperature T at a time t will differ from T for the case of no neutrino heating. So for the rest of this chapter, quantities will be graphed

Set of Graphs	Condition
5	Full neutrino heating
6	Change in f_{ν_i} only
7	Change in T only
8	e^+, e^- scattering excluded
9	e^+e^- annihilation excluded
10	$\nu_i\nu_j$ reactions excluded
14	Heating with MB Statistics
16	$m_e = 0.0$, FD Statistics
17	$m_e = 0.0$, MB Statistics

Table 3.2: The conditions of the run that corresponds to each set of graphs.

vs. the time t in seconds. For comparison the borders on the top will feature T corresponding to time t for the case of no neutrino heating. All runs in this chapter use the list of 1781 timestep values generated from the full neutrino heating run.

3.4.1 Full Neutrino Heating

Figure (3.5a) shows the change in the weak reaction rates that convert neutrons to protons

$$\begin{aligned} n + \nu_{\rm e} &\rightarrow p + {\rm e}^- \\ n + {\rm e}^+ &\rightarrow p + \bar{\nu}_{\rm e} \\ n &\rightarrow p + {\rm e}^- + \bar{\nu}_{\rm e} \end{aligned}$$

for the case of full neutrino heating. Neutrino heating leads to more energetic neutrinos, and less energetic electrons and positrons. So the electron neutrinos can be more tightly coupled to the neutrons in the reaction n + $\nu_{\rm e} \rightarrow$ p + e$^-$, but the positrons are less tightly coupled to the neutrons in the reaction n +

$e^+ \rightarrow p + \bar{\nu}_e$. Thus Figure (3.5a) shows an increase the rate for $n + \nu_e \rightarrow p + e^-$ but a decrease for $n + e^+ \rightarrow p + \bar{\nu}_e$. (In these graphs increases are indicated with a solid line and decreases are indicated with a long dash line.) The change in the rates start out nearly five orders of magnitude smaller than the rates themselves. By the time t of around 3.0 seconds $f_{\nu_e}(p)$ has increased significantly due to neutrino heating. At that time the change in the rates are only two orders of magnitude smaller than the rates themselves. Also, the increase of $n + \nu_e \rightarrow p + e^-$ starts out nearly equal to the decrease of $n + e^+ \rightarrow p + \bar{\nu}_e$. But $e^- e^+$ annihilation depletes the positrons, and the change in the rate for $n + e^+ \rightarrow p + \bar{\nu}_e$ gradually lags behind the change for $n + \nu_e \rightarrow p + e^-$. So the total change in the rate of neutron to proton conversion is always an increase, starting out an order of magnitude less than the changes for the invidual rates but ultimately being nearly equal to the change for $n + \nu_e \rightarrow p + e^-$.

Figure (3.5b) shows the change in the proton to neutron conversion rates, the reverse directions of the reactions listed above. The same features found in Figure (3.5a) are found here as well. The rate for $p + \bar{\nu}_e \rightarrow n + e^+$ increases while the rate for $p + e^- \rightarrow n + \nu_e$ decreases. The changes of both rates are nearly equal until when the decrease in the rate for $p + e^- \rightarrow n + \nu_e$ noticibly declines due to the depletion of electrons. So here again, the reaction with ν_e on its left side has the larger change, and the change is an increase. This increase eventually dominates the total increase in the proton to neutron conversion rates, though the change turns negative at around 20 seconds because the rate for $p + \bar{\nu}_e \rightarrow n + e^+$ falls more rapidly than the rate for $p + e^- \rightarrow n + \nu_e$. But at this time the conversion rates have fallen out of equilibrium, and so the proton to neutron reactions are no

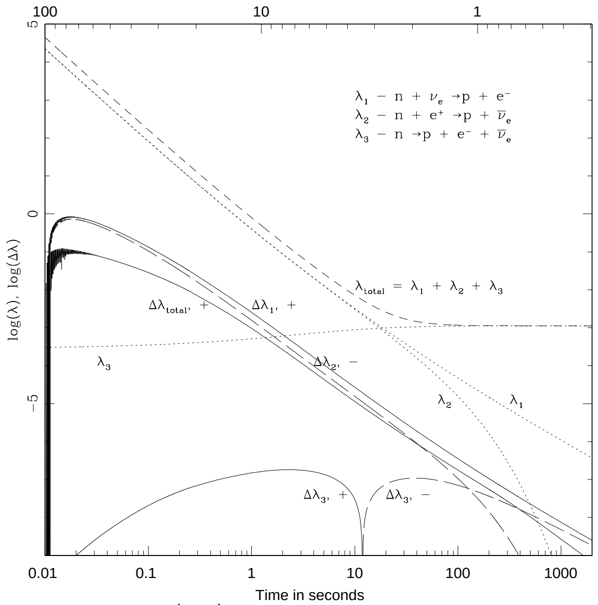

(3.5a): Change in in n →p Rates

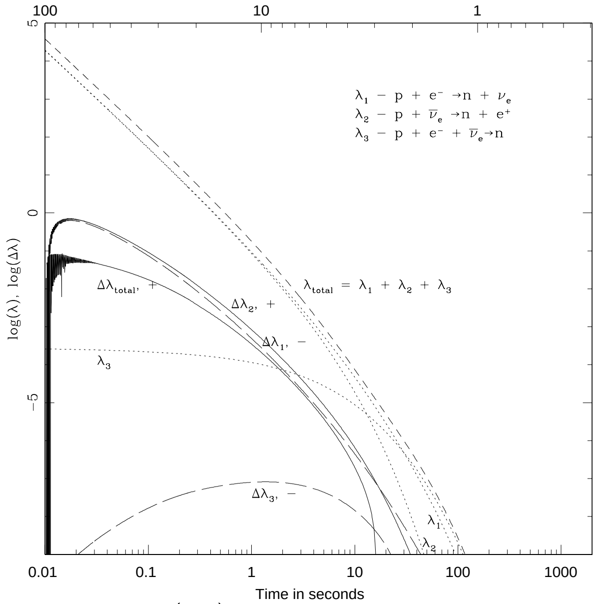

(3.5b): Change in in p →n Rates

Figure 3.5: The changes in the n/p conversion rates and the mass fractions for free neutrons and ^{4}He for the case of full neutrino heating.

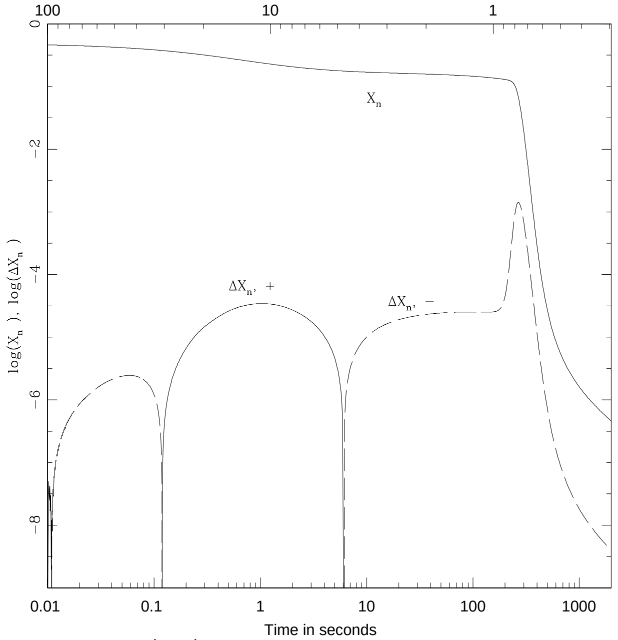

(3.5c): Change of Neutron Mass Fraction

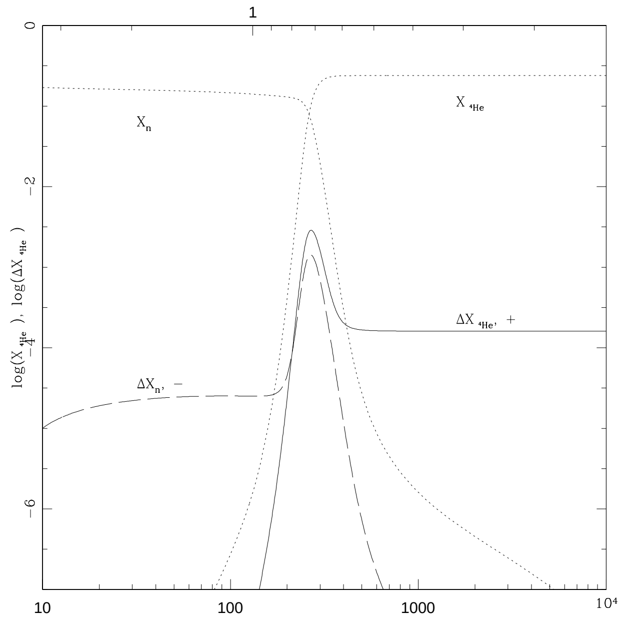

(3.5d): Change of ^{4}He Mass Fraction

longer signficant. The total increase in the proton to neutron rates turns out to always be significantly smaller than the increase in the neutron to proton rates.

The conversion reactions occur more rapidly in both directions, bringing the neutrons and protons closer to equilibrium with each other. When they're closer to equilibrium the amount of neutrons should increase. Figure (3.5c) shows the mass fraction X_{n} of free neutrons and the change ΔX_{n} due to full neutrino heating. For a time period of around 0.1 s. to 10 s., when the conversion rates are starting to decouple, X_{n} has a net increase. The increase in X_{n} is reflected in the increase in neutron decay $\mathrm{n} \to \mathrm{p} + \mathrm{e}^{-} + \bar{\nu}_{\mathrm{e}}$ shown in Figure (3.5a). But by 10 s. the proton to neutron reactions have fallen to considerably lower values than the neutron to proton reactions. The increased neutron to proton rates eventually deplete X_{n} so that from 10 s on X_{n} is lower than for the case of no heating. Likewise the neutron decay rate decreases in Figure (3.5a), but by then the decrease is smaller in proportion to the decay rate itself.

In the meantime the mass fraction $X_{^4\mathrm{He}}$ has always had a slight increase due to neutrino heating. Increased interaction between neutrons and protons leads to an increase in the amount of free neutrons and protons that get used in nuclear reactions. Nuclear reactions depend on both the baryon energy density ρ_b and the temperature T. The Texas code determines T from $\rho_{\mathrm{e}+\gamma}$, which is reduced by neutrino heating. So at any set time t the temperature will be lower. Likewise, at any set temperature T the time will be earlier than in the case with no heating. So Big Bang Nucleosynthesis occurs earlier in the case with heating than without when T reaches to around 0.8 GK, an effect known as the clock effect. Figure (3.5d) shows X_{n} and $X_{^4\mathrm{He}}$, and the decrease

ΔX_{n} in neutrons and the increase $\Delta X_{^4\mathrm{He}}$ in ^{4}He due to heating. When the nuclear reactions become significant $\Delta X_{^4\mathrm{He}}$ becomes comparable in magnitude to ΔX_{n}. So the graph for ΔX_{n} has a peak wherein free neutrons are being rapidly incorporated ultimately into ^{4}He molecules. The peak has its top at the time when X_{n} falls below $X_{^4\mathrm{He}}$. The graph for $X_{^4\mathrm{He}}$ levels off earlier than in the case with no neutrino heating. In the time when $X_{^4\mathrm{He}}$ with heating has levelled off but $X_{^4\mathrm{He}}$ without heating would still be increasing the graph for $\Delta X_{^4\mathrm{He}}$ has a dip. In the time when $X_{^4\mathrm{He}}$ is constant with or without heating $\Delta X_{^4\mathrm{He}}$ levels off to a final value of 1.60×10^{-4}.

3.4.2 The effects of $f_{\nu_{\mathrm{e}}}$ and T

This author tries to illustrate how the increase in $f_{\nu_{\mathrm{e}}}$ and the decrease in T individually affect a runs results in the Figures (3.6a-d) and (3.7a-d). The results for Figures (3.6a-d) correspond to the case where $f_{\nu_{\mathrm{e}}}$ changes but not T. This author drops the final term in Equation (3.1), and in Equation (2.9) this author uses the value ρ_ν has when there's no heating. Therefore while $f_{\nu_{\mathrm{e}}}$ can still increase from heating the means that neutrino heating can change T, either by changing $\rho_{\mathrm{e}+\gamma}$ or by changing the timestep evolution through $\ln R$, have been disabled. Figures (3.6a) and (3.6b) show the resulting changes on the conversion rates. The increases in the rates for $\mathrm{n} + \nu_{\mathrm{e}} \to \mathrm{p} + \mathrm{e}^-$ and $\mathrm{p} + \bar{\nu}_{\mathrm{e}} \to \mathrm{n} + \mathrm{e}^+$ are comparable to the increases in Figures (3.5a) and (3.5b). But the decreases in the rates for $\mathrm{n} + \mathrm{e}^+ \to \mathrm{p} + \bar{\nu}_{\mathrm{e}}$ and $\mathrm{p} + \mathrm{e}^- \to \mathrm{n} + \nu_{\mathrm{e}}$ are now two orders of magnitude smaller. The $[1-f_{\nu_{\mathrm{e}}}(p)]$ term in the integrands cannot have as large an effect on these rates as the change in T would have. With the decreases in those particular rates reduced the total increases $\Delta\lambda(\mathrm{n} \to \mathrm{p})$

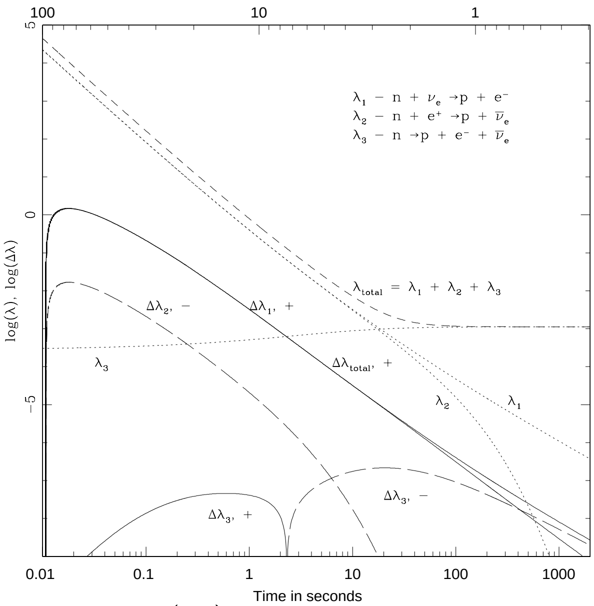

(3.6a): Change in in n →p Rates

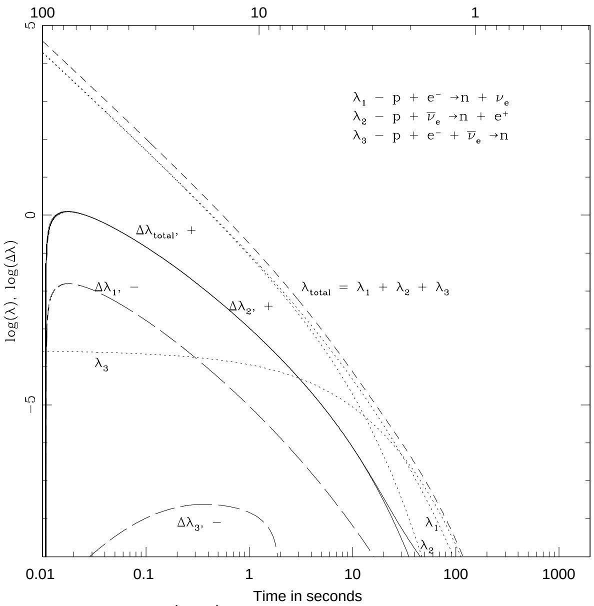

(3.6b): Change in in p →n Rates

Figure 3.6: The changes in the n/p conversion rates and the mass fractions for free neutrons and ^{4}He for the case when heating changes only the neutrino distribution functions.

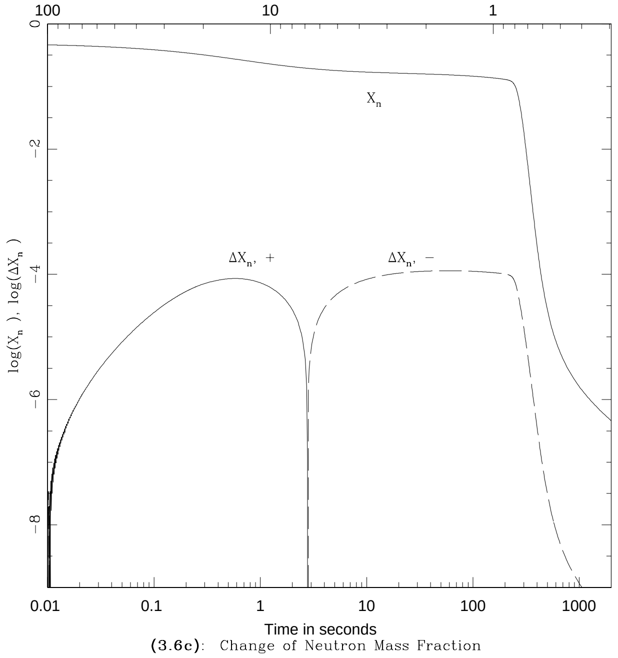

(3.6c): Change of Neutron Mass Fraction

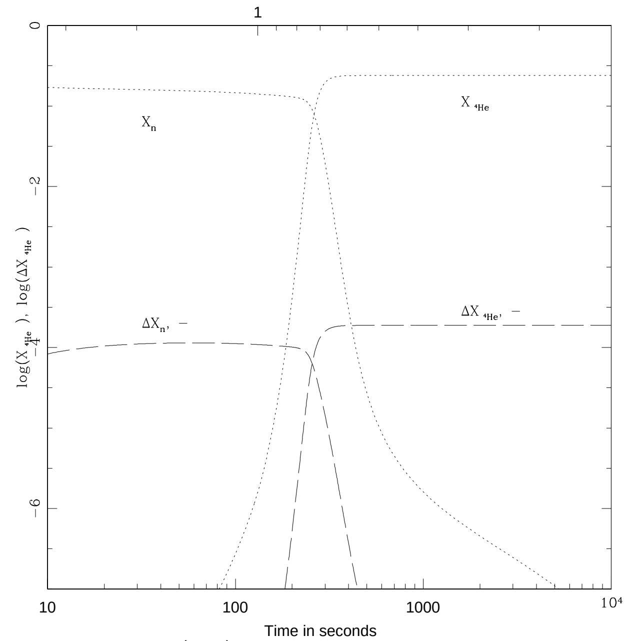

(3.6d): Change of ^{4}He Mass Fraction

and $\Delta\lambda(\mathrm{p} \to \mathrm{n})$ are larger than in Figures (3.5a) and (3.5b). (The increases are also larger because f_{ν_e} are larger in the case of heating where T doesn't change than for full neutrino heating. The electrons and positrons are more energetic. So when they interact with the neutrinos they increase ρ_{ν_e} and ρ_{ν_μ} by greater amounts, 1.01 % and 0.504 % respectively.)

The neutrons and protons are more coupled when heating changes only f_{ν_e} than in the case of full neutrino heating. As shown in Figure (3.6c) the stronger coupling results in a larger increase ΔX_n in the neutron mass fraction, and an increase right from the start. But the faster rate of converting neutrons to protons overcomes this positive ΔX_n at around 3.0 s, leading to a greater decrease in X_n than for full neutrino heating. Since T is the same as for without heating, the nuclear reaction rates are the same as in the case without heating, and the time of nucleosynthesis doesn't change. So when nucleosynthesis occurs it occurs with fewer neutrons than for the case without heating. $\Delta X_{^4\mathrm{He}}$ turns negative also at 3.0 s., and stays negative for the rest of the run. Figure (3.6d) shows no peak in the graphs as this case has no clock effect. ΔX_n and $\Delta X_{^4\mathrm{He}}$, both negative, simply track the graphs of X_n and $X_{^4\mathrm{He}}$. $\Delta X_{^4\mathrm{He}}$ has a final value of -1.89 $\times 10^{-4}$.

For Figures (3.7a) and (3.7b) this author instead modifies the calculations of the conversion rates so that they use the Fermi-Dirac values of f_{ν_e} instead of the actual heated value. So T is allowed to decrease but f_{ν_e} isn't allowed to change the conversion rates. This modification has the opposite effect on Figures (3.7a) and (3.7b) that the modification for Figures (3.6a) and (3.6b) had. The rates for $\mathrm{n} + \mathrm{e}^+ \to \mathrm{p} + \bar{\nu}_\mathrm{e}$ and $\mathrm{p} + \mathrm{e}^- \to \mathrm{n} + \nu_\mathrm{e}$ decrease about as much as in Figures (3.5a) and (3.5b), but this time the rates for $\mathrm{n} + \nu_\mathrm{e} \to \mathrm{p} + \mathrm{e}^-$ and $\mathrm{p} + \bar{\nu}_\mathrm{e} \to \mathrm{n} + \mathrm{e}^+$ fall two orders of magnitude. In this case then the overall conversion rates between neutrons and protons decrease.

Since only the conversion rates have been modified from the full neutrino heating case the reactions between the neutrinos and the electrons and positrons will not be affected, and ρ_{ν_e} and ρ_{ν_μ} will increase by the same amount as in the case of full heating. Rather, the modifications will only affect the final values of the isotope abundances. Figure (3.7c) shows that changing T has the opposite effect on X_n that changing f_{ν_e} has. With the conversion rates decreased instead of increased the neutrons and protons start out less coupled than for the case of no heating, and ΔX_n starts out negative. When only the neutron to proton reactions are important ΔX_n changes to positive due to the slower rate of depleting neutrons. But $n + \nu_e \rightarrow p + e^-$ and $p + \bar{\nu}_e \rightarrow n + e^+$ are also affected by $e^- e^+$ annihilation. So the magnitudes of ΔX_n aren't as great as in Figure (3.6c). Since T is allowed to fall due to heating this run has a clock effect making nucleosynthesis occur earlier. The clock effect combines with the positive value for ΔX_n to lead to a $\Delta X_{^4\mathrm{He}}$ that's always positive and larger in magnitude to $\Delta X_{^4\mathrm{He}}$ for the case of full neutrino heating. Figure (3.7d) shows how ΔX_n is positive right up to when nucleosynthesis starts, and then the excess neutrons are more rapidly converted than in the case for full heating. The final value of $\Delta X_{^4\mathrm{He}}$ is 3.11×10^{-4}, nearly twice as much in magnitude as that for the case when only f_{ν_e} changes. This large magnitude comes from how the decrease in T both slows down the neutron/proton conversion rates and makes nucleosynthesis occur earlier and faster. One can see how the increase in f_{ν_e} and the decrease in T can combine to yield the resulting values of ΔX_n and $\Delta X_{^4\mathrm{He}}$ shown in Figures (3.5c) and (3.5d).

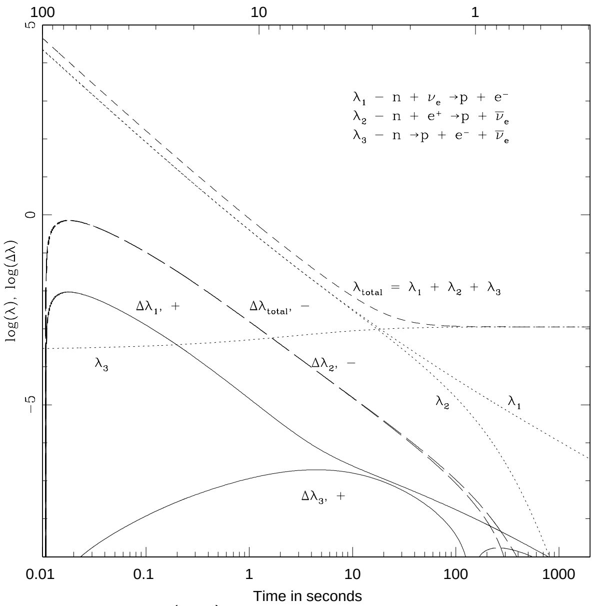

(3.7a): Change in in n →p Rates

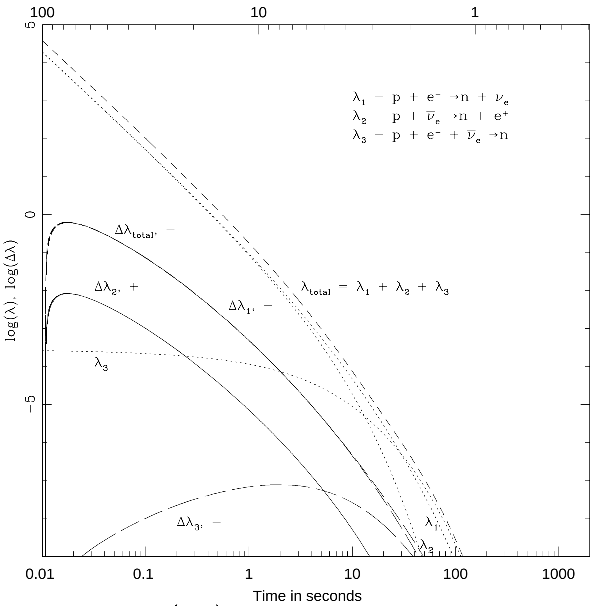

(3.7b): Change in in p →n Rates

Figure 3.7: The changes in the n/p conversion rates and the mass fractions for free neutrons and ^{4}He for the case when heating only makes the ($e^{\pm} + \gamma$) temperature T decrease.

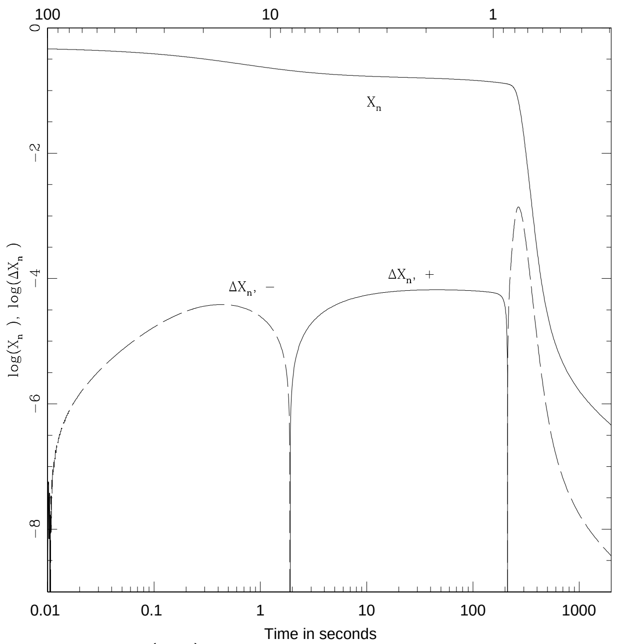

(3.7c): Change of Neutron Mass Fraction

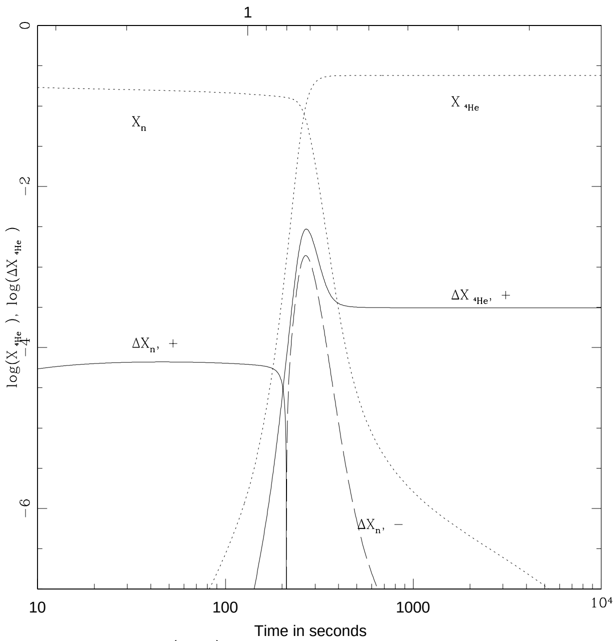

(3.7d): Change of ^{4}He Mass Fraction

3.4.3 The Effect of e^-e^+ Annihilation, e^-, e^+ Scattering, and $\nu_i\nu_j$ Reactions

Figure (3.3) shows the changes in ρ_{ν_e} and ρ_{ν_μ} when either supress e^-, e^+ scattering, e^-e^+ annihilation, or $\nu_i\nu_j$ reactions are suppressed from neutrino heating. The sets of Figures (3.8) to (3.10) show the changes in the conversion rates, X_n and $X_{^4He}$ corresponding to these cases.

Figures (3.8a-d) correspond to the case of no e^-, e^+ scattering. In Figures (3.8a) and (3.8b) the graphs for the increases in the neutron to proton rates and the proton to neutron rates appear to be the same as in Figures (3.5a) and (3.5b). In fact the values in (3.8a) and (3.8b) are smaller. Smaller by around 13 % for the increase in neutron to proton rates at time $t = 1$ second, and as much as 30 % for the proton to neutron rates at that time. But the scale of (3.8a) and (3.8b) is such that one can barely see the differences between (3.8b) and (3.5b) and not see the differences between (3.8a) and (3.5a) at all. Still the reduced increase of f_{ν_e} due to the absense of e^-, e^+ scattering leads to reduced increases in the conversion rates, felt more on the proton to neutron rates than the neutron to proton rates.

In Figure (3.8c) ΔX_n is positive more briefly than in Figure (3.5c) because the conversion rates haven't increased as much in this case. In the time when ΔX_n is negative the increase in the proton to neutron rates is much more reduced than the neutron to proton rates. The negative ΔX_n then has a larger magnitude than in the case of full neutrino heating. Figure (3.3) shows that ρ_{ν_e} doesn't increase as much when e^-, e^+ scattering is left out, and likewise $\rho_{e+\gamma}$ and T are larger at a given time for the case without e^-, e^+ scattering than with. But the reduction of the increase is slight. The absence of e^-, e^+

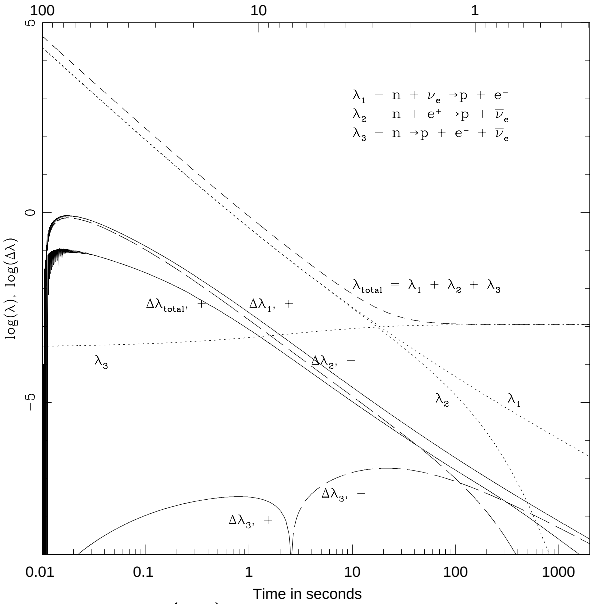

(3.8a): Change in in n →p Rates

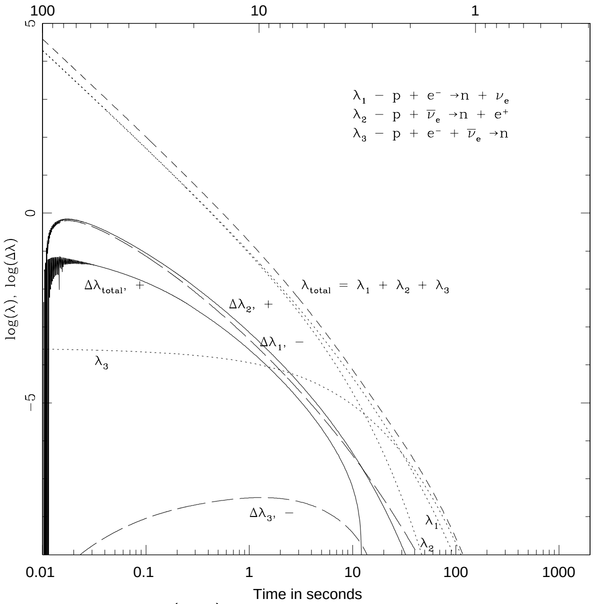

(3.8b): Change in in p →n Rates

Figure 3.8: The changes in the n/p conversion rates and the mass fractions for free neutrons and ^{4}He for the case when no neutrino scattering off of e^-, e^+ occurs.

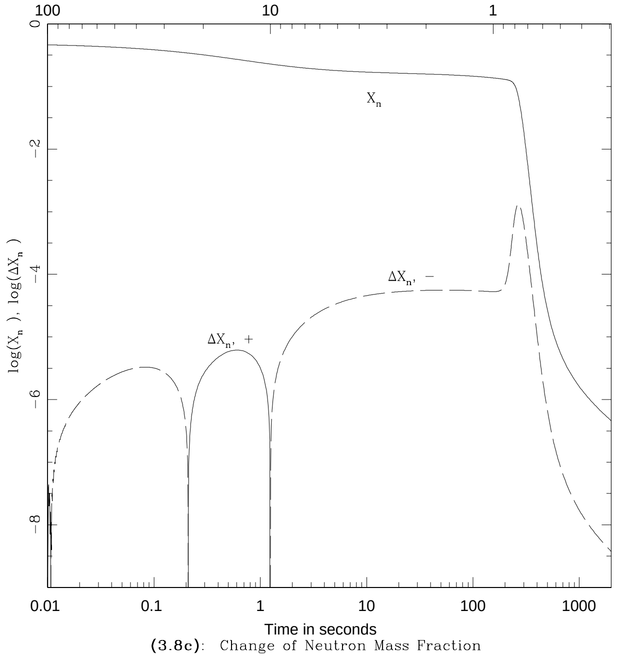

(3.8c): Change of Neutron Mass Fraction

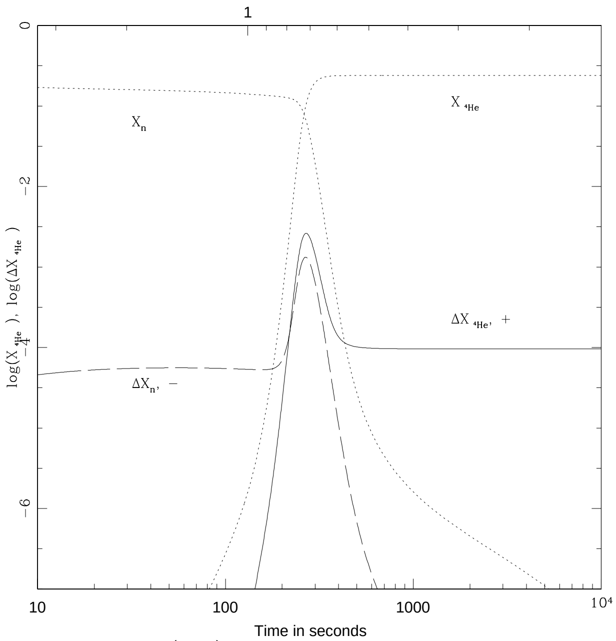

(3.8d): Change of ^{4}He Mass Fraction

scattering then shouldn't affect the decrease in T as much as the increase in f_{ν_e}. Figure (3.8d) shows $\Delta X_{^4\mathrm{He}}$ for this case. $\Delta X_{^4\mathrm{He}}$ starts out less by around 8 % than for full heating, a difference not perceptable in the scale of (3.5d) and (3.8d). But once over the peak $\Delta X_{^4\mathrm{He}}$ decreases to a considerably lower final value of 0.958 $\times 10^{-4}$, 40 % lower than the 1.60×10^{-4} increase for full heating. Because T isn't as severely affected as f_{ν_e} the clock effect is reduced, and the rates that destroy ^{4}He might be destroying the lowered amount of ^{4}He nearly as rapidly as before. So $X_{^4\mathrm{He}}$ settles on a lower value.

When $\mathrm{e}^-\mathrm{e}^+$ annihilation is left out ρ_{ν_e} and ρ_{ν_μ} increase only slightly, and likewise $\rho_{e+\gamma}$ and T decrease slightly. As a result the increase in the rate for n + $\nu_e \rightarrow$ p + e^- and the decrease for n + $\mathrm{e}^+ \rightarrow$ p + $\bar{\nu}_e$ shown in Figure (3.9a) are noticibly lower in magnitude than in Figure (3.5a). The absence of $\mathrm{e}^-\mathrm{e}^+$ conversion to $\nu_i\bar{\nu}_i$ pairs seems to affect the rates more drasticly through the change in T than in f_{ν_e}, and the decrease for n + $\mathrm{e}^+ \rightarrow$ p + $\bar{\nu}_e$ is reduced more than the increase n + $\nu_e \rightarrow$ p + e^-. The changes in these two rates don't cancel each other out as precisely as for the case of full neutrino heating. The overall increase in the neutron to proton conversion rate starts out larger in Figure (3.9a) than in Figure (3.5a), before eventually becoming considerably smaller. In Figure (3.9b) the decrease in p + $\mathrm{e}^- \rightarrow$ n + ν_e and the increase in p + $\bar{\nu}_e \rightarrow$ n + e^+ are likewise reduced, but moreso for p + $\mathrm{e}^- \rightarrow$ n + ν_e than for p + $\bar{\nu}_e \rightarrow$ n + e^+. As a result the net increase in the proton to neutron conversion rate is only slightly smaller from the rate for the case of full neutrino heating.

The increase in the proton to neutron conversion rate is slightly changed while the increase in the neutron to proton conversion rate is considerably reduced. In Figure (3.9c) ΔX_{n} winds up positive for the whole time when

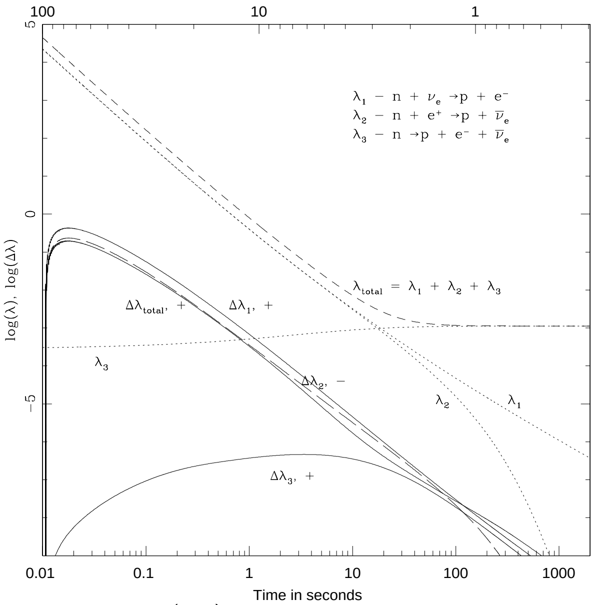

(3.9a): Change in in n →p Rates

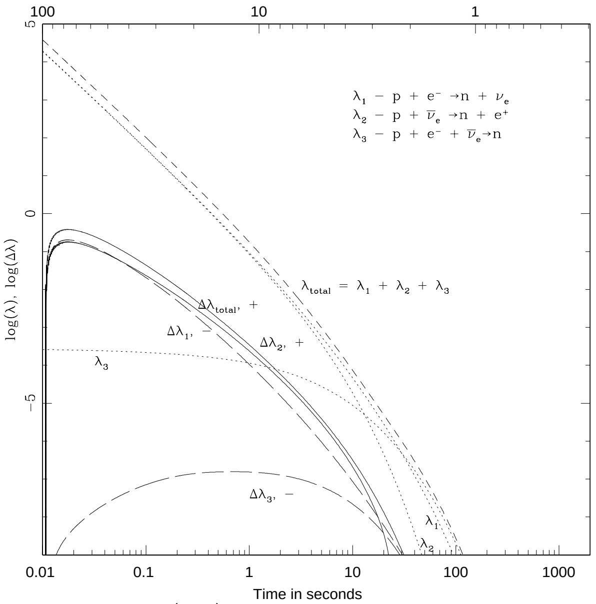

(3.9b): Change in in p →n Rates

Figure 3.9: The changes in the n/p conversion rates and the mass fractions for free neutrons and ^{4}He for the case when no e^-e^+ annihilation occurs.

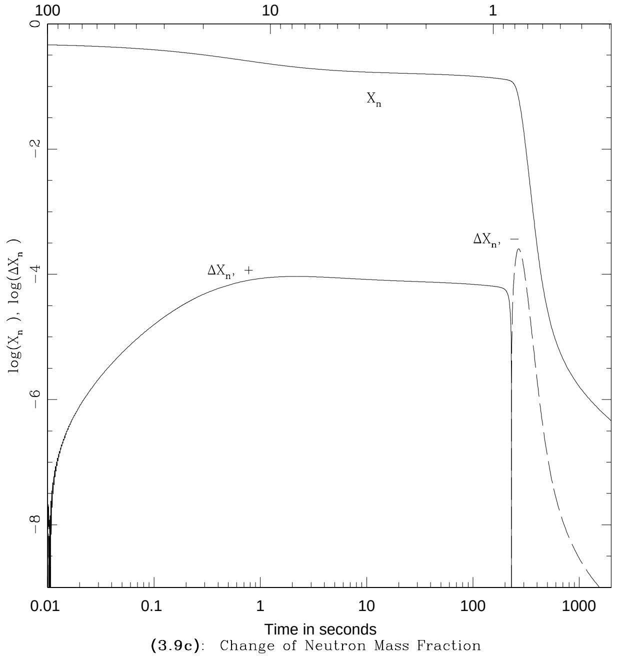

(3.9c): Change of Neutron Mass Fraction

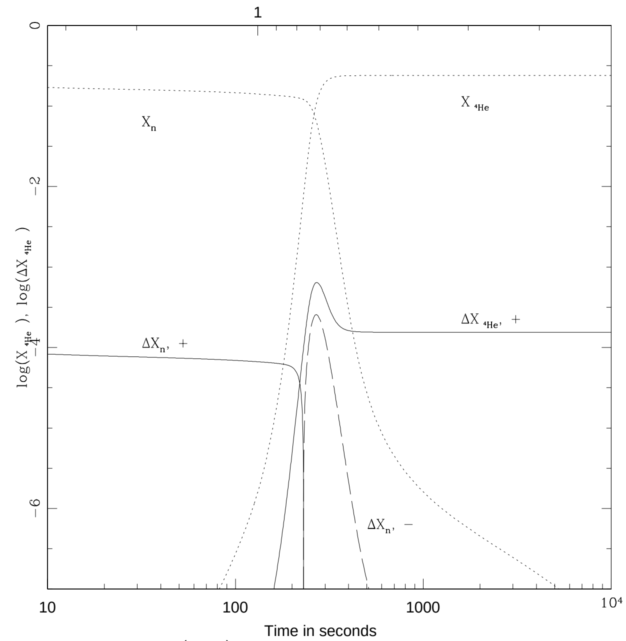

(3.9d): Change of ^{4}He Mass Fraction

the conversion rates are significant. Since for the case of no e^-e^+ annihilation T at a given time decreases only slightly, at a given T the nuclear reaction rates are not as increased here as in the case of full neutrino heating, and nucleosynthesis doesn't begin as early. In Figure (3.9d) $\Delta X_{^4\mathrm{He}}$ is positive, but at first not as large in magnitude as in Figure (3.5d). But when $\Delta X_{^4\mathrm{He}}$ starts falling the reactions that destroy ^{4}He are not running as rapidly as they are in (3.5d). Surprisingly enough, $\Delta X_{^4\mathrm{He}}$ has a final value nearly equal to its value for full heating, 1.54 $\times 10^{-4}$.

Figures (3.10a-d) correspond to the case when the reactions between neutrinos are left out. The increase in ρ_{ν_e} in this case is larger than in the case of full heating by about as much as it is smaller in the case for no e^-, e^+ scattering, but the increase in ρ_{ν_μ} is smaller. The changes in the neutron to proton conversion rate and the proton to neutron conversion rate turn out also to increase in magnitude by as much as they decrease for the case of no e^-, e^+ scattering, by 13 % at time $t = 1$ second for the neutron to proton rate and 35 % for the proton to neutron rate. The increase in f_{ν_e} causes the conversion reactions with neutrinos on their left hand sides to increase while, as in the case for no e^-, e^+ scattering, the reactions with electrons or positrons on the left hand sides are relatively unchanged.

The increases in conversion rates make the neutrons and protons more tightly coupled. In Figure (3.10c) ΔX_{n} is positive for a slightly larger region of time, and when it turns negative it has a larger magnitude than in Figure (3.5c). But the decrease in T is nearly for the case of no neutrino-only reactions as for the case of full heating, maybe because the decrease of $\Delta\rho_{\nu_\mu}$ cancels out the increase of $\Delta\rho_{\nu_e}$. So as shown in Figure (3.10d) the final value of $\Delta X_{^4\mathrm{He}}$ is only slightly smaller than in the case of full heating, at 1.44 $\times 10^{-4}$.

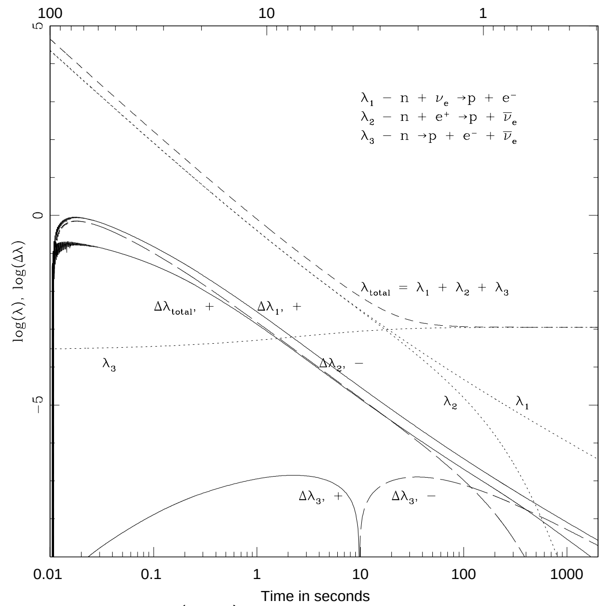

(3.10a): Change in in n →p Rates

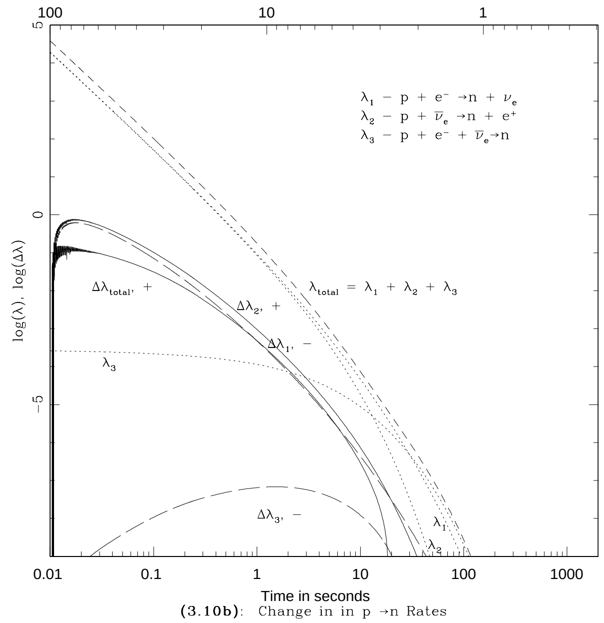

(3.10b): Change in in p →n Rates

Figure 3.10: The changes in the n/p conversion rates and the mass fractions for free neutrons and ^{4}He for the case when no $\nu_i\nu_j$ reactions occur.

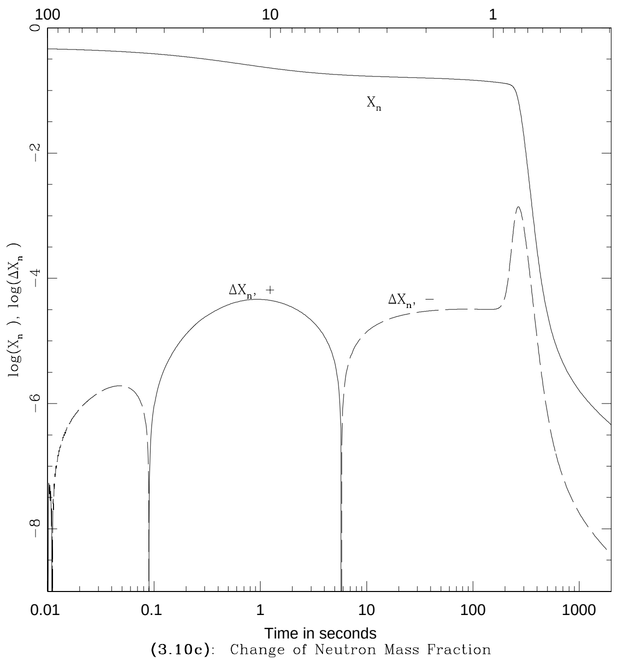

(3.10c): Change of Neutron Mass Fraction

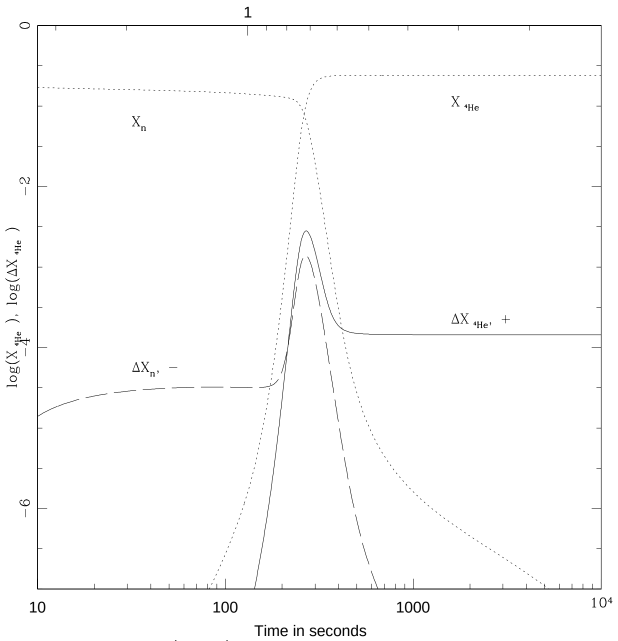

(3.10d): Change of ^{4}He Mass Fraction

3.4.4 The Effect of Maxwell-Boltzmann Statistics and of the Value of m_{e}

As stated in Section (3.2) papers such as those written by Fields, Dodelson and Turner ([30], [31]) simplify the calculation of the neutrino heating effect by using Maxwell-Boltzmann statistics

$$f_{\mathrm{MB}}(E) \;=\; \frac{1}{e^{E/kT}}$$

in the Boltzmann Transport Equation. The phase-space factor in Equation (3.4) then simplifies to:

$$\Lambda(f_1, f_2, f_3, f_4) \;=\; f_3(p_3)f_4(p_4) - f_1(p_1)f_2(p_2)$$

If all the distributions in this version of Λ equal f_{MB} then Λ will equal zero. Section (3.3) notes that using the Maxwell-Boltzmann version of Λ greatly simplifies Equation (3.7). In order to produce consistent data the Texas code has to use Maxwell-Boltzmann statistics everywhere. The neutrinos, the electrons and positrons, even the photons have to obey Maxwell-Boltzmann statistics. So the following thermal quantities have to change.:

$$\begin{aligned}
\rho_{\gamma\mathrm{MB}} &= \frac{90}{\pi^4}aT^4 \\
\rho_{\mathrm{eMB}} &= \frac{30}{\pi^4}aT^4\int_0^\infty dX\frac{X^2\sqrt{X^2+E^2}}{e^{\sqrt{X^2+E^2}}} \\
P_{\mathrm{eMB}} &= \frac{10}{\pi^4}aT^4\int_0^\infty dX\frac{X^4}{\sqrt{X^2+E^2}(e^{\sqrt{X^2+E^2}})} \\
N_{\mathrm{eMB}} &= \frac{30}{k\pi^4}aT^3\int_0^\infty dX\frac{X^2}{e^{\sqrt{X^2+E^2}}}
\end{aligned}$$

$$\rho_{\nu\mathrm{MB}} = \frac{90}{\pi^4} a T_\nu^4$$

At the highest temperatues ρ_{eMB} equals $(90/\pi^4)aT^4$, the same as $\rho_{\gamma\mathrm{MB}}$. So $\mathrm{e^-e^+}$ annihilation raises T to $3^{1/3}T_\nu$ rather than $(11/4)^{1/3}T_\nu$. The present-day neutrino temperature $T_{\nu_o} = 1.890$ K then, and the expansion rate $R = T_{\nu_o}/T_\nu$ is smaller. The equations for the neutron-proton conversion rates have to change as well.

$$\begin{aligned}
\lambda(\mathrm{n} + \nu_\mathrm{e} \to \mathrm{p} + \mathrm{e}^-, \mathrm{MB}) &= \frac{1}{\tau_\mathrm{n}\lambda_0} \int v_\mathrm{e} E_\mathrm{e}^2 p_{\nu_\mathrm{e}}^2 dp_{\nu_\mathrm{e}} f_{\nu_\mathrm{e}} \\
\lambda(\mathrm{n} + \mathrm{e}^+ \to \mathrm{p} + \bar{\nu}_\mathrm{e}, \mathrm{MB}) &= \frac{1}{\tau_\mathrm{n}\lambda_0} \int p_{\nu_\mathrm{e}}^2 p_\mathrm{e}^2 dp_\mathrm{e} f_\mathrm{e} \\
\lambda(\mathrm{p} + \mathrm{e}^- \to \mathrm{n} + \nu_\mathrm{e}, \mathrm{MB}) &= \frac{1}{\tau_\mathrm{n}\lambda_0} \int p_{\nu_\mathrm{e}}^2 p_\mathrm{e}^2 dp_\mathrm{e} f_\mathrm{e} \\
\lambda(\mathrm{p} + \bar{\nu}_\mathrm{e} \to \mathrm{n} + \mathrm{e}^+, \mathrm{MB}) &= \frac{1}{\tau_\mathrm{n}\lambda_0} \int v_\mathrm{e} E_\mathrm{e}^2 p_{\nu_\mathrm{e}}^2 dp_{\nu_\mathrm{e}} f_{\nu_\mathrm{e}} \\
\lambda(\mathrm{p} + \mathrm{e}^- + \bar{\nu}_\mathrm{e} \to \mathrm{n}, \mathrm{MB}) &= \frac{1}{\tau_\mathrm{n}\lambda_0} \int v_\mathrm{e} p_{\nu_\mathrm{e}}^2 E_\mathrm{e}^2 dp_{\nu_\mathrm{e}} f_{\nu_\mathrm{e}} f_\mathrm{e}
\end{aligned}$$

In Maxwell-Boltzmann statistics, the integral in the equation for $\lambda(n \to p + e^- + \bar{\nu}_e)$ always equals λ_0. So $\lambda(n \to p + e^- + \bar{\nu}_e) = 1/\tau_n$ always.

Figure (3.11) compares the Maxwell-Boltzmann conversion rates vs. the Fermi-Dirac rates, for the cases of no neutrino heating. Both electron neutrinos and electrons/positrons are represented by the larger Maxwell-Boltzmann distribution functions. So the overall neutron to proton rate and the overall proton to neutron rate, and in fact the individual rates listed above, get increased, considerably more than the increases from the heating effect. The increased conversion rates mean more neutrons get converted to protons. So X_n is lower in the case of Maxwell-Boltzmann statistics than in Fermi-Dirac

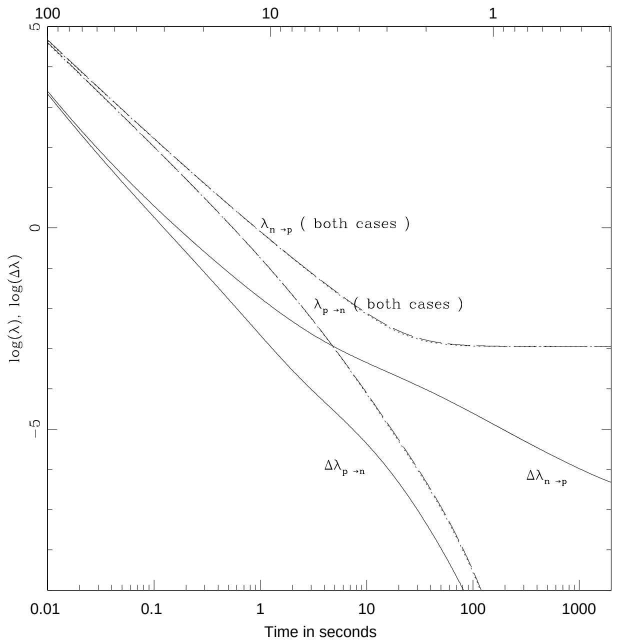

Figure 3.11: The n/p conversion rates are much greater when using Maxwell-Boltzmann statistics instead of Fermi-Dirac statistics.

statistics for the whole run until nucleosynthesis occurs. The electromagnetic plasma energy density $\rho_{e+\gamma}$ is larger for Maxwell-Boltzmann statistics. The temperature T is larger at a given time as well. So nucleosynthesis occurs at a later time than for Fermi-Dirac statistics, and at a given T the nuclear reaction rates will be slower. Figure (3.12) shows that the final value for $X_{^4\mathrm{He}}$ is lower for Maxwell-Boltzmann statistics: 0.22985 vs. 0.23907. The decrease in $X_{^4\mathrm{He}}$ alone is larger in magnitude than the any changes in $X_{^4\mathrm{He}}$ from neutrino heating.

In Figure (3.13) the solid lines correspond to the fractional increases in ρ_{ν_e} and ρ_{ν_μ} for the case of Fermi-Dirac statistics while the long-dashed lines are for Maxwell-Boltzmann statistics. The Fermi-Dirac increases are normalized to

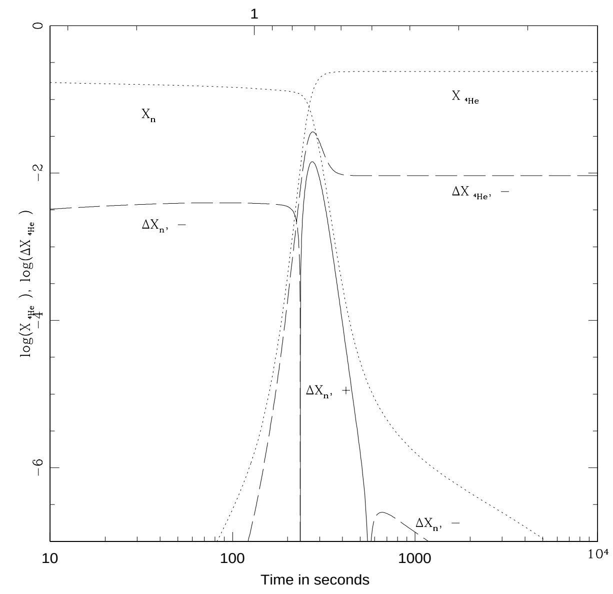

Figure 3.12: Fewer neutrons and a later time for nucleosynthesis leads to a smaller value of $X_{^4\mathrm{He}}$ when using MB statistics.

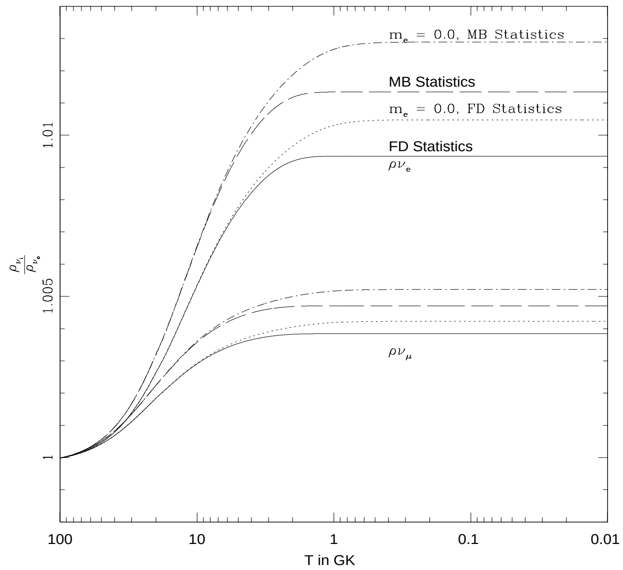

Figure 3.13: Larger distribution functions lead to larger increases in ρ_{ν_e} and ρ_{ν_μ} at all times. Setting m_e to zero increases f_e and increases ρ_{ν_e} and ρ_{ν_μ} further at later times.

the Fermi-Dirac expressions for ρ_{ν_e} and ρ_{ν_μ} with no heating while the Maxwell-Boltzmann increases are normalized to the corresponding Maxwell-Boltzmann expressions. The larger Maxwell-Boltzmann distribution functions make both the neutrinos and the electrons and positrons more abundant. So more energy is transferred to neutrinos in the Maxwell-Boltzmann case, and ρ_{ν_e} and ρ_{ν_μ} increase by 1.134 % and 0.471 % respectively. The difference between the type of statistics used influences the results right from the beginning.

Figures (3.14a) and (3.14b) show the changes in the neutron/proton conversion rates due to neutrino heating, in relation to the conversion rates for the case of Maxwell-Boltzmann statistics and no heating. Figure (3.14a) has no $\Delta\lambda(\mathrm{n} \to \mathrm{p} + \mathrm{e}^- + \bar{\nu}_\mathrm{e})$ because neutrino heating doesn't change neutron decay for Maxwell-Boltzmann statistics. The larger distribution functions raise in magnitude both the increases of the rates for $\mathrm{n} + \nu_\mathrm{e} \to \mathrm{p} + \mathrm{e}^-$ and $\mathrm{p} + \bar{\nu}_\mathrm{e} \to \mathrm{n} + \mathrm{e}^+$ and the decreases of the rates for $\mathrm{n} + \mathrm{e}^+ \to \mathrm{p} + \bar{\nu}_\mathrm{e}$ and $\mathrm{p} + \mathrm{e}^- \to \mathrm{n} + \nu_\mathrm{e}$, resulting in larger increases for the total neutron to proton conversion rate and the proton to neutron conversion rate (9.6 % more for the neutron to proton conversion rates at time $t = 1$ second, and 13 % more for the proton to neutron conversion rates at that time).

The graph for the change in X_n shown in Figure (3.14c) has the same behavior for Maxwell-Boltzmann statistics as for Fermi-Dirac statistics. Whether positive or negative, the magnitudes of ΔX_n are slightly larger for Maxwell-Boltzmann statistics reflecting the larger increases in the conversion rates. Figure (3.14d) shows the decrease in X_n and the increase in $X_{^4\mathrm{He}}$ at around the time of nucleosynthesis. At a given time, the temperature T will be smaller with heating than without. But with heating or without, T will be larger for Maxwell-Boltzmann statistics than for Fermi-Dirac statistics. Therefore Big-

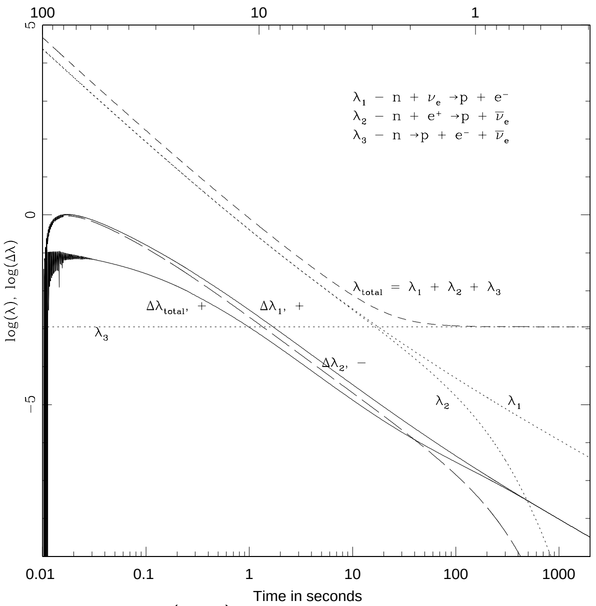

(3.14a): Change in in n →p Rates

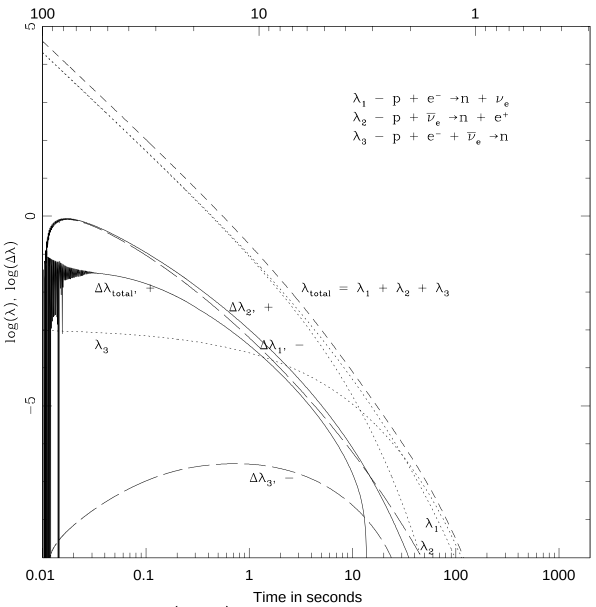

(3.14b): Change in in p →n Rates

Figure 3.14: The changes in the n/p conversion rates and the mass fractions for free neutrons and ^{4}He for the case of neutrino heating using Maxwell-Boltzmann statistics.

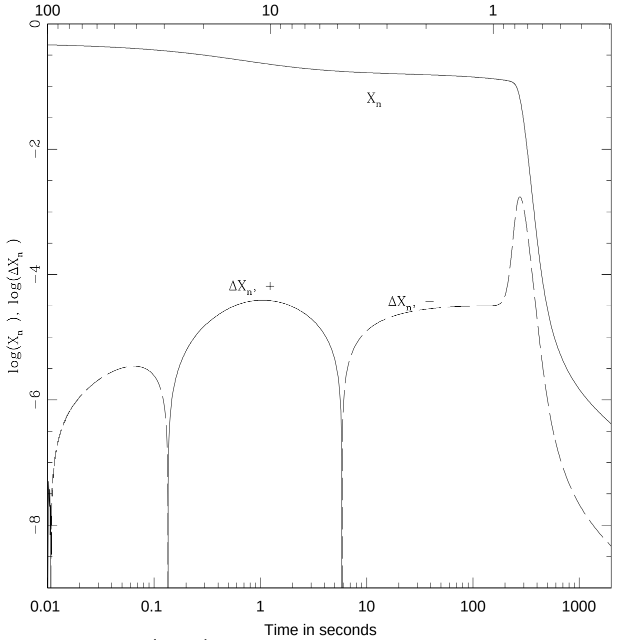

(3.14c): Change of Neutron Mass Fraction

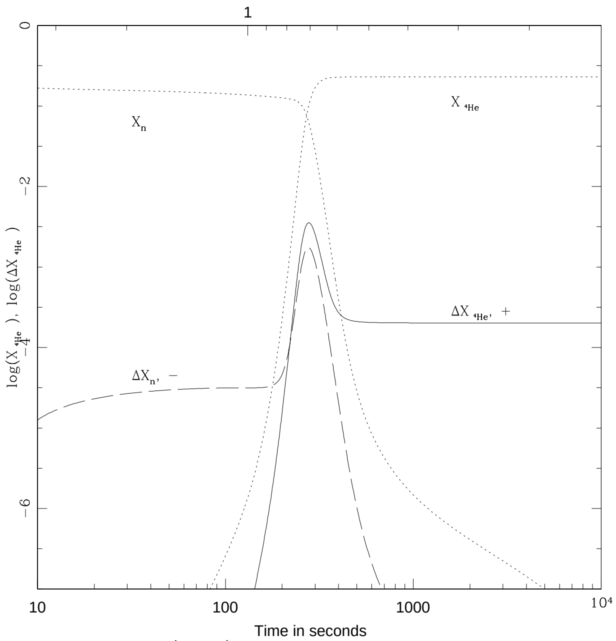

(3.14d): Change of ^{4}He Mass Fraction

Bang Nucleosynthesis will occur later for the Maxwell-Boltzmann case. In (3.14d), the graph for $\Delta X_{^4\mathrm{He}}$ peaks at a later time, and so attains a larger magnitude before it starts to decrease. So for Maxwell-Boltzmann statistics $\Delta X_{^4\mathrm{He}}$ has a higher final value, 2.01 $\times 10^{-4}$ vs. 1.60 $\times 10^{-4}$.

To further simplify the Boltzmann Transport Equation, Fields, Dodelson and Turner set the electron mass m_e to zero in this equation. But the Boltzmann Equation is the **only** part of their code where they set m_e to zero. Figure (3.13) shows the increase of ρ_{ν_e} and ρ_{ν_μ} with $m_\mathrm{e} = 0.0$ as well as without for both Fermi-Dirac and Maxwell-Boltzmann statistics, and Figures (3.15) show the increases of the electron neutrino distribution function $f_{\nu_\mathrm{e}}(p)$ for $m_\mathrm{e} = 0.0$. Comparing (3.15a) with (3.1a), the graphs for $f_{\nu_\mathrm{e}}(p_i)$ start out the same. But at $T = 6$ GK, kT nearly equals the electron mass. Here the graphs in (3.1a) and (3.15a) start to diverge, with the graphs for $m_\mathrm{e} = 0.0$ increasing more rapidly than for nonzero m_e. Note the equation for the Fermi-Dirac distribution function of electrons. For Fermi-Dirac statistics $f_\mathrm{e}(p = 0.0) = 1/[\exp(m_\mathrm{e}/T) + 1]$, which goes lower and lower as T decreases, while $f_{\nu_\mathrm{e}}(p = 0.0) = 0.5$ always. So in the Boltzmann equation for $\mathrm{e}^-\mathrm{e}^+$ annihilation f_e can't keep up with f_{ν_e} and so the prevailing direction changes from $\nu_\mathrm{e} + \bar{\nu}_\mathrm{e} \to \mathrm{e}^- + \mathrm{e}^+$ to $\mathrm{e}^- + \mathrm{e}^+ \to \nu_\mathrm{e} + \bar{\nu}_\mathrm{e}$. But f_e can keep up with f_{ν_e} if $m_\mathrm{e} = 0.0$. So in Figure (3.15a) all the graphs keep increasing far beyond the graphs in (3.1a) until they asymptote, instead of the highest graphs decreasing for nonzero m_e. Likewise in Figure (3.13) the graphs for ρ_{ν_e} and ρ_{ν_μ} for $m_\mathrm{e} = 0.0$ start to diverge from the graphs for nonzero m_e at around 6 GK and take a longer time to asymptote. The final % increases is higher for both types of statistics (1.010 % and 0.423 % for Fermi-Dirac Statistics and 1.289 % and 0.522 % for Maxwell-Boltzmann Statistics).

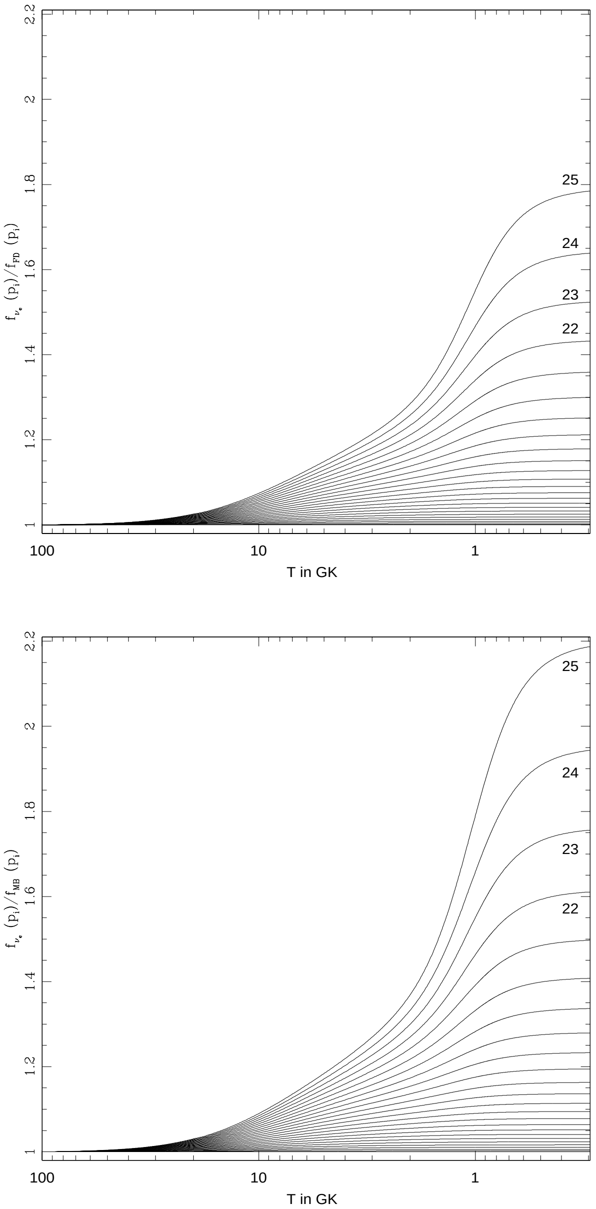

Figure 3.15: The fractional increases of f_{ν_e} using Fermi-Dirac Statistics (3.15a) and Maxwell-Boltzmann statistics (3.15b) when $m_e = 0$. f_{ν_e} for the highest momenta don't decrease like they due in Figure (3.1a).

Figures (3.16a) and (3.16b) show that the changes in the neutron-proton conversion rates behave as one would expect when $m_{\mathrm{e}} = 0.0$. For the highest temperatures there's no difference between the conversion rates whether m_{e} is zero or not. But at around 3 seconds when T is around 6 GK in both scenarios, the overall increases in the proton to neutron conversion rates and the neutron to proton conversion rates in (3.16a) and (3.16b) start to diverge upward from the increases in (3.5a) and (3.5b). But this divergence is very slight (imperceptible in the graphs' scale.), and at a time when the conversion rates don't have much influence on the results anymore. The graph for ΔX_{n} in Figure (3.16c) greatly resembles that in Figure (3.5c), with ΔX_n being no more than 1 % larger in magnitude with $m_{\mathrm{e}} = 0.0$ than without. Since $\rho_{\nu_{\mathrm{e}}}$ and ρ_{ν_μ} are larger by the time T reaches 1 GK nucleosynthesis should begin earlier. In Figure (3.16d) the peak of $\Delta X_{^4\mathrm{He}}$ is higher than in the case of nonzero m_{e}, leading to a slightly larger final value of 1.79 $\times 10^{-4}$.

Figures (3.17a-d) correspond to the case of neutrino heating with $m_{\mathrm{e}} = 0.0$ and using Maxwell-Boltzmann statistics. The behavior of the graphs is the same as the case for Fermi-Dirac statistics. The increases in the neutron to proton conversion rates and the proton to neutron conversion rates are larger in (3.17a) and (3.17b) than in (3.15a) and (3.15b), but only after T falls below 6 GK, and only slightly larger. Nucleosynthesis occurs later in Figure (3.17d) than in (3.15d). So the peak in (3.17d) is higher and the final value of $\Delta X_{^4\mathrm{He}}$ is slightly higher, from 2.01 $\times 10^{-4}$ to 2.27 $\times 10^{-4}$. Maxwell-Boltzmann Statistics and $m_{\mathrm{e}} = 0.0$ are the conditions used by Fields, Dodelson, and Turner, and those conditions yield a value of $\Delta X_{^4\mathrm{He}}$ that's 41 % larger than the 1.60 $\times 10^{-4}$ that this author gets using the true conditions of nonzero m_{e} and Fermi-Dirac Statistics.

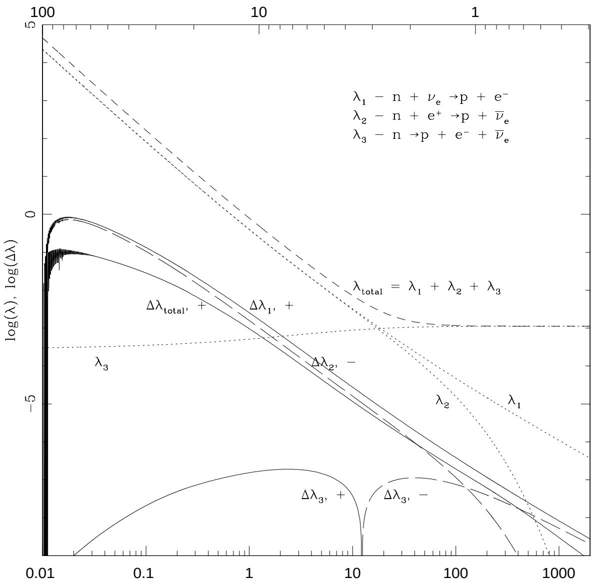

(3.16a): Change in in n →p Rates

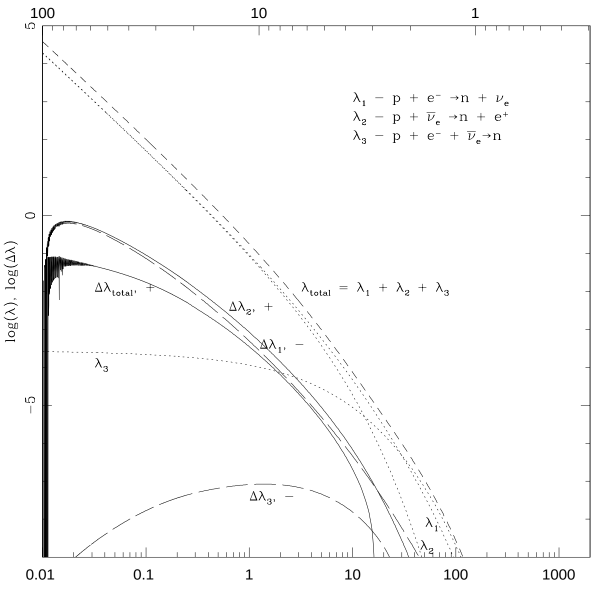

(3.16b): Change in in p →n Rates

Figure 3.16: The changes in the n/p conversion rates and the mass fractions for free neutrons and ^{4}He for the case of $m_e = 0$ and Fermi-Dirac Statistics.

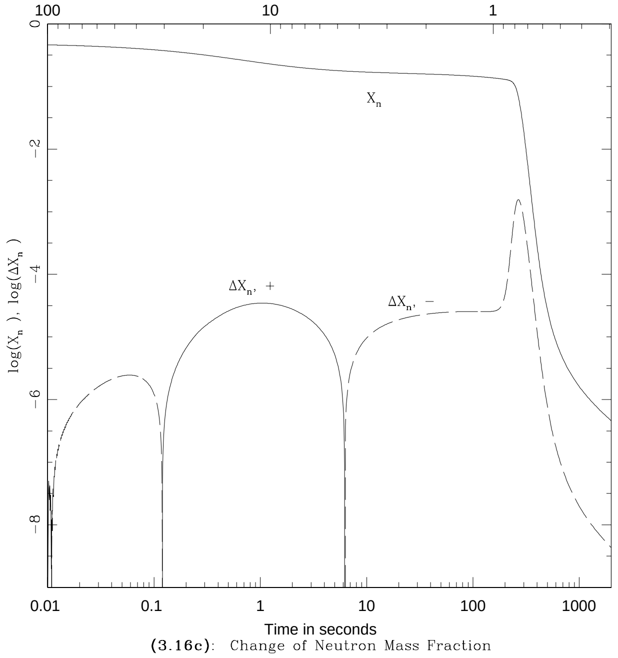

(3.16c): Change of Neutron Mass Fraction

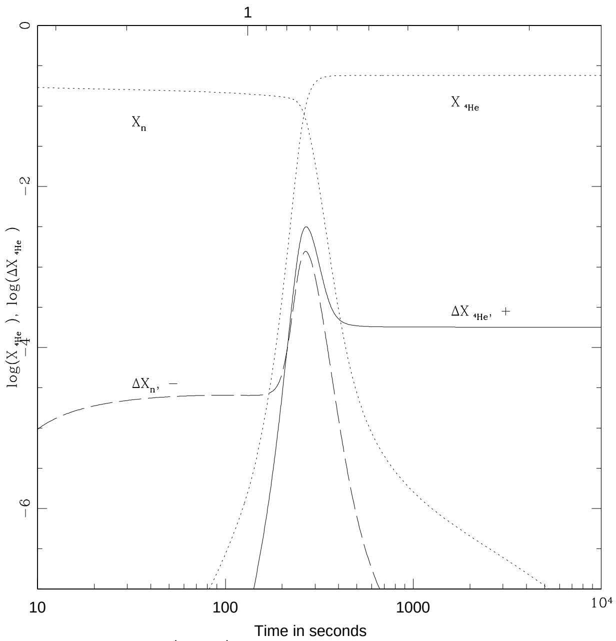

(3.16d): Change of ^{4}He Mass Fraction

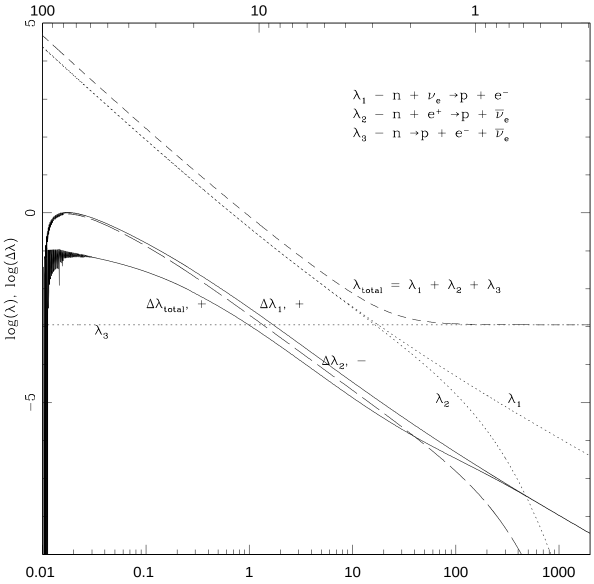

(3.17a): Change in in n →p Rates

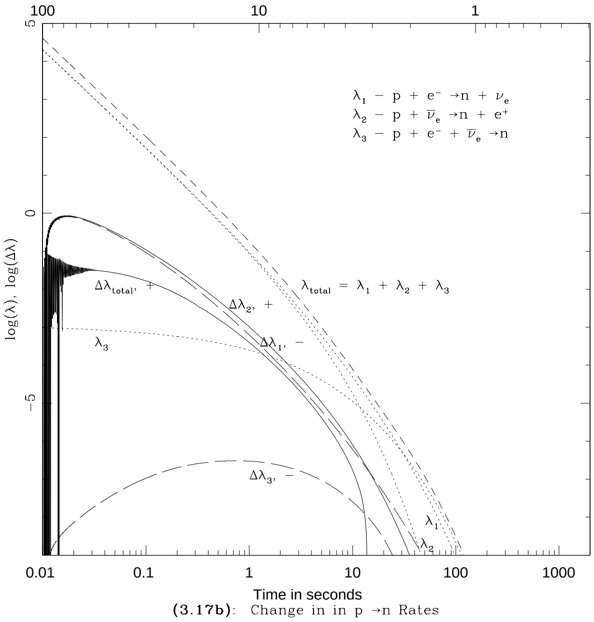

(3.17b): Change in in p →n Rates

Figure 3.17: The changes in the n/p conversion rates and the mass fractions for free neutrons and ^{4}He for the case of $m_{\mathrm{e}} = 0$ and Maxwell-Boltzmann Statistics.

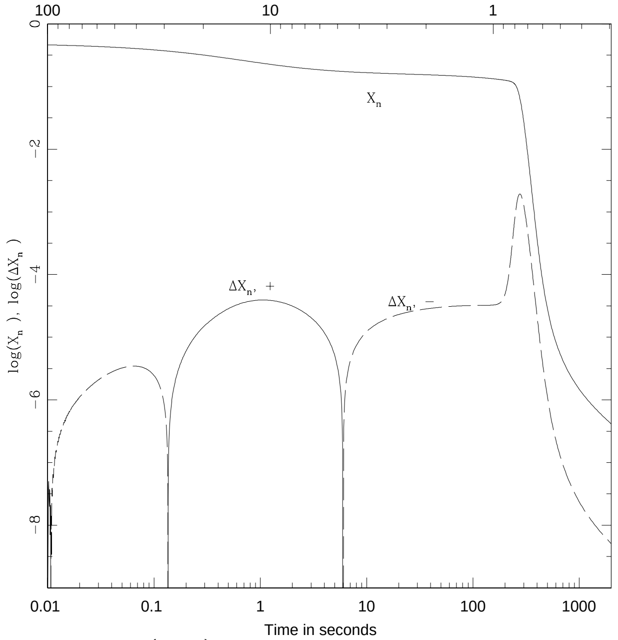

(3.17c): Change of Neutron Mass Fraction

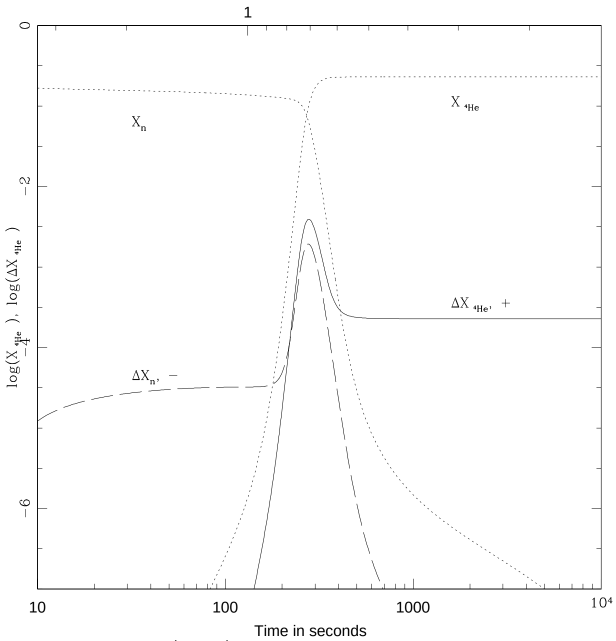

(3.17d): Change of ^{4}He Mass Fraction

Condition	ρ_{ν_e} % Increase	ρ_{ν_μ} % Increase
FD, Full Heating	0.935	0.384
Only f_{ν_i} Changes	1.012	0.504
Only T Changes	0.935	0.384
No e^-, e^+ Scattering	0.863	0.353
No e^-e^+ Annihilation	0.158	0.091
No $\nu_i\nu_j$ Reactions	1.020	0.322
$m_e = 0.0$	1.010	0.423
MB, Full Heating	1.134	0.471
MB, $m_e = 0.0$	1.289	0.522

Table 3.3: The % increases of ρ_{ν_i} for all the conditions discussed in this chapter. The last two cases in each table are compared to results for Maxwell-Boltzmann statistics and no heating. In all cases $\eta_{10} = 3.0$.

3.4.5 Summary of Results

Table (3.3) lists the % increases of ρ_{ν_e} and ρ_{ν_μ} for all nine of the conditions the Texas code was run with the neutrino heating effect on (Remember that $\rho_{\nu_\tau} = \rho_{\nu_\mu}$), and Table (3.4) lists the final mass fractions $X_{^4\mathrm{He}}$ of ^{4}He for all the cases. Chiefly through annihilation into neutrino pairs the electrons and positrons transfer energy to the neutrinos, and the neutrinos distribute the energy between the three species via interactions with each other. The small magnitudes of the increases reflect the fact that most energy from e^-e^+ annihilation transfers to photons instead of neutrinos, and the smaller magnitude for muons and τ particles reflects the fact that electron neutrinos can have both charged current and neutral current interactions with electrons and positrons. Heating increases the distribution functions of the neutrinos, increasing the neutron/proton conversion rates that start with electron neutrinos. These increased rates lead to a lower mass fraction X_n of free neutrons. That condition on its own would lead to a decrease in $X_{^4\mathrm{He}}$, as shown in the results where

Condition	$X_{^4\mathrm{He}}$	$\Delta X_{^4\mathrm{He}}$
FD, No Heating	0.239070694	
FD, Full Heating	0.239231116	1.604 $\times 10^{-4}$
Only f_{ν_i} Changes	0.238882020	-1.887 $\times 10^{-4}$
Only T Changes	0.239381827	3.111 $\times 10^{-4}$
No e^-, e^+ Scattering	0.239166484	0.958 $\times 10^{-4}$
No e^-e^+ Annihilation	0.239225099	1.544 $\times 10^{-4}$
No $\nu_i\nu_j$ Reactions	0.239214467	1.438 $\times 10^{-4}$
$m_\mathrm{e} = 0.0$	0.239249823	1.791 $\times 10^{-4}$
MB, No Heating	0.229858854	
MB, Full Heating	0.230060336	2.015 $\times 10^{-4}$
MB, $m_\mathrm{e} = 0.0$	0.230085900	2.270 $\times 10^{-4}$

Table 3.4: The final values of $X_{^4\mathrm{He}}$ and (where applicable) $\Delta X_{^4\mathrm{He}}$ for all the conditions discussed in this chapter. $\Delta X_{^4\mathrm{He}}$ for Maxwell-Boltzmann cases are compared with the value of $X_{^4\mathrm{He}}$ for Maxwell-Boltzmann statistics and no heating. In all cases $\eta_{10} = 3.0$.

only f_{ν_i} changes. But the electrons and positrons' loss of energy also lowers the electromagnetic plasma temperature T, lowering the conversion rates that start out with e^- or e^+. A lower T also leads to an earlier onset of Big Bang Nucleosynthesis, and faster nuclear reaction rates when BBN occurs. These effects tend to increase $X_{^4\mathrm{He}}$, and are more significant at the time of nucleosynthesis then the effects from f_{ν_e}.

It can be difficult to predict exactly what final value of $X_{^4\mathrm{He}}$ comes from the combination of these effects, though. For the three cases when certain reactions between neutrinos and electrons/positrons were left out, the results in Table (3.3) are simple to explain. But the results in Table (3.4) vary unusually. Leaving out e^-, e^+ scattering has a small effect on the neutrino energy densities and a noticible effect on the increase in ^{4}He. Leaving out e^-e^+ annihilation greatly reduces the increase of the energy densities, but the final increase in ^{4}He is nearly unchanged from the case of full neutrino heating.

This author has had to trace through the changes in the conversion rates and the neutron abundance to try to explain these nonobvious results.

The Texas code was also run using simplifications to the neutrino heating calculation used in other articles. For instance this dissertation shows results with electron mass m_e set to zero in the Boltzmann Transport Equation, but only in that equation. That condition has a significant effect on the increases of the neutrino energy densities, and can fundamentally alter the evolution of the neutrino distribution functions. But a zero m_e has a small effect on the increase of the ^{4}He mass fraction, increasing $\Delta X_{^4\mathrm{He}}$ by only around 10 %. Whereas when one uses Maxwell-Boltzmann Statistics the larger distribution functions of both the neutrinos and the electrons/positrons and the greater increase in T from $\mathrm{e}^-\mathrm{e}^+$ annihilation into photon pairs lead to a 25 % increase of $\Delta X_{^4\mathrm{He}}$, and the neutrino energy densities have larger increases as well. This dissertation's results mimic the behavior reported in (HM, 1995) [32] and (DT, 1992) [30], where the former's energy density and ^{4}He mass fraction increases were smaller than the latter's because they used Fermi-Dirac statistics and nonzero m_e. The dissertation's magnitudes tend to be larger. (1.6 $\times 10^{-4}$ vs. 1.1 $\times 10^{-4}$ from (HM, 1995), and 2.3 vs. 1.5 from (DT, 1992)). For the Texas code to work using Maxwell-Boltzmann statistics, the densities of the photons, electrons and positrons, and neutrinos and the conversion rates all have to be converted to Maxwell-Boltzmann statistics. The value of $X_{^4\mathrm{He}}$ itself using Maxwell-Boltzmann statistics differs from $X_{^4\mathrm{He}}$ using Fermi-Dirac statistics more greatly than $X_{^4\mathrm{He}}$ from any of the conditions with neutrino heating on. As the Texas code can be run using the correct conditions of Fermi-Dirac statistics and nonzero m_e, the simplifications from previous papers now seem unnecessary.

isotope	No Heating	Full Heating
n	$0.5265615284 \times 10^{-15}$	$0.5204237826 \times 10^{-15}$
p	0.7607704301	0.7606104021
d	$0.122053476 \times 10^{-3}$	$0.1217110721 \times 10^{-3}$
^{3}He	$0.3623227123 \times 10^{-4}$	$0.3618281792 \times 10^{-4}$
^{3}H	$0.5898346918 \times 10^{-6}$	$0.5883098768 \times 10^{-6}$
^{4}He	0.2390706937	0.2392311151
^{6}Li	$0.1458101815 \times 10^{-12}$	$0.1455393433 \times 10^{-12}$
^{7}Li	$0.3436667153 \times 10^{-9}$	$0.3431491548 \times 10^{-9}$
^{7}Be	$0.2778895818 \times 10^{-9}$	$0.2795772597 \times 10^{-9}$
^{9}Be	$0.1087415056 \times 10^{-16}$	$0.1082963879 \times 10^{-16}$
^{10}B	$0.9381505231 \times 10^{-18}$	$0.9362589543 \times 10^{-18}$
^{11}B	$0.9628963674 \times 10^{-16}$	$0.9788624885 \times 10^{-16}$
^{12}C	$0.3005922125 \times 10^{-13}$	$0.3024338105 \times 10^{-13}$
^{13}C	$0.2042492263 \times 10^{-14}$	$0.2060403236 \times 10^{-14}$
^{14}C	$0.6491689417 \times 10^{-13}$	$0.6520053532 \times 10^{-13}$
^{14}N	$0.13166241 \times 10^{-12}$	$0.1321594669 \times 10^{-12}$
^{16}O	$0.7611748737 \times 10^{-17}$	$0.7665152008 \times 10^{-17}$
^{19}F	$0.7443152836 \times 10^{-24}$	$0.7475464814 \times 10^{-24}$
^{20}F	$0.3514904424 \times 10^{-24}$	$0.3496674817 \times 10^{-24}$
^{21}Ne	$0.5345445903 \times 10^{-23}$	$0.5384753665 \times 10^{-23}$

Table 3.5: Mass fractions for the case of no neutrino heating compared with the mass fractions for full neutrino heating and Fermi-Dirac statistics. $\eta_{10} = 3.0$.

Finally Table (3.5) lists the Texas code's mass fractions for various isotopes for both with neutrino heating and without. Like with $X_{^4\mathrm{He}}$ the changes in the mass fractions tend to be 10^{-4} smaller in magnitude than the mass fractions themselves. The mass fractions of isotopes such as deuterium and ^{7}Li which peak and decrease to their final values tend to decrease due to neutrino heating, while the mass fractions that don't peak such as ^{4}He and ^{7}Be tend to increase. Nuclear reactions are faster at the time of nucleosynthesis, and so perhaps the isotopes of the first kind get destroyed more rapidly while those of the second kind get created more rapidly. In comparison to the change in mass fractions due to the increase in the number of timesteps, the change due to neutrino heating is usually three times larger.

3.5 Neutrino Electron Plasma Instability

The equations for C_{coll} used in this chapter were for the case of the neutrinos having mass $m_\nu = 0.0$ The electron mass m_{e} is nonzero in C_{coll}. The expressions involving m_{e} can serve as an outline for rederiving C_{coll} with nonzero neutrino masses. The distribution functions $f_{\nu_{\mathrm{e}}}$, f_{ν_μ}, and f_{e} are homogeneous and isotropic. Giving unspecified spatial or directional dependences to $f_{\nu_{\mathrm{e}}}$ and f_{ν_μ} would add other variables that would have to be evaluated numerically, multiplying the code's run time considerably. If the inhomogeneity or anisotropy obeys a known well behaved equation though than one might still be able to integrate over the new spatial/directional variables analytically. One has to look at specific examples.

In his doctoral dissertation [41] Chi-hsuan Lai of the University of Texas at Austin discusses the phenomenon of neutrino electron plasma instability, which could lead to inhomogeneous distributions of the neutrinos, electrons and positrons. Neutrinos undergo electroweak reactions with electrons and positrons for temperatures $T = 12$ TK and lower. Using nonzero neutrino masses, Lai couples the classical hydrodynamical equations that describes electron/positron and neutrino fluids and their mutual interaction with Maxwell's equations, and solves the equations for perturbations of n_{e} and n_{ν_i} from their equilibrium values and the fields $\delta\vec{E}$ and $\delta\vec{B}$ from zero. n_{e}, n_{ν_i}, $\delta\vec{E}$ and $\delta\vec{B}$ are written in Fourier space. Solving Maxwell's equations for $\delta\vec{E}(\omega, \vec{k})$ yields:

$$0 = \Lambda_{ij}\delta E_j(\omega, \vec{k})$$

Setting the determinant of the matrix equations Λ_{ij} to zero leads to two independent dispersion relations. The solutions to these relations turn out to be unstable, separating the neutrinos from the electrons and positrons.

Neutrino electron plasma instability can be applied to supernovae. A star collapses forming a core of neutrinos ("neutrino stars") and an outer layer of electrons, positrons and photons. Electroweak interactions can lead to plumes of neutrinos diffusing into the outer layer. The instability causes the plumes to rapidly expand outward. This rapid expansion would be an explosion in the supernova model. This scenario is interesting because most simulations of supernovae don't have explosions worked in. But Lai felt that in the Big Bang the time frame for the temperatures needed for this instability was too small for the instability to have a significant effect on the results of Big Bang Nucleosynthesis.